GE Nuclear Energy

NEDC-32288
Revision 0
Class 2
November 1993

Scaling of the SBWR Related Tests

G. Yadigaroglu*

Reviewed: _____

J.R. Fitch
Testing & Performance Analysis
SBWR Project

Reviewed: _____

T.R. McIntyre, Manager
Testing & Performance Analysis
SBWR Project

Approved: _____

P.W. Marriott, Manager
SBWR Project

*Professor of Nuclear Engineering, Swiss Federal Institute of Technology (ETH), Zurich, Switzerland.

DISCLAIMER OF RESPONSIBILITY

This document was prepared for the General Electric Company (GE). No other use, direct or indirect, of the document or the information it contains is authorized; and with respect to any unauthorized use, neither GE or any of the contributors to this document makes any representation or warranty (express or implied) as to the completeness, accuracy, or usefulness of the information contained in this document or that such use of such information may not infringe privately owned rights; nor do they assume any responsibility for liability or damage of any kind which may result from such use of such information. Furnishing this document does not convey any license, express or implied, to use any patented invention or any information of GE disclosed herein, or any rights to publish or make copies of the document without prior written permission of GE.

Table of Contents

List of Tables

List of Figures

ACKNOWLEDGMENTS

The author is indebted to GE Nuclear Energy staff members P. Billig, F. Moody, and A. Rao, for providing valuable assistance, information and comments on drafts of this report, and in particular to J. Fitch for numerous thoughtful comments, insights, and suggestions for improvements, which have been incorporated in this report. Thanks are extended to M. Swope for editorial assistance.

He is also indebted for comments on drafts of this report to J. Healzer of S. Levy, Inc. and for information regarding the PANDA facility to PSI staff members J. Dreier, M. Huggenberger, and G. Varadi.

P. Coddington and M. Meier of PSI, in collaboration with M. Andreani (Swiss Federal Institute of Technology, ETH in Zurich) provided unpublished material regarding scaling of various phenomena and useful comments.

Nomenclature and Abbreviations

Nomenclature

A	Surface area [m^2]
a	Cross-sectional area [m^2]
c_p	Specific heat at constant pressure [J/kg K]
c_v	Specific heat at constant volume [J/kg K]
D	Diameter [m]
E	Internal energy [J]
e	Specific internal energy [J/kg]
f	Friction factor
F	See Equation 2.27
F_n	See Equation 2.26
H	Height [m]
h	Specific enthalpy [J/kg]
h_{fg}	Latent heat of vaporization [J/kg]
g	Acceleration of gravity [9.81 m/s^2]
j	Volumetric flow rate [m^3/s]
k	Ratio of specific heats, c_p/c_v
l	Length [m]
L	Sum of lengths [m]
M	Mass [kg]
$\dot{M}$	Flow rate [kg/s]
p	Pressure [Pa]
$\dot{Q}$	Heat addition rate [W]
R	Universal gas constant [J/kg K]
R	System scale
T	Temperature [K]
t	Time [s]
u	Velocity [m/s]
V	Volume [m^3]
v	Specific volume [kg/m^3]
y	Mass fraction
z	Axial coordinate [m]
δ	Kronecker delta
μ	Viscosity

Π	Non–dimensional number
ρ	Density [kg/m^3]
σ	Surface tension
τ	Time constant [s]
ω	Characteristic frequency [s^{-1}]

Subscripts

G	Gas
L	Liquid
LG	Change liquid to gas
R	Scaling factor between prototype and model

Additional subscripts are defined in the text

Superscripts

+	Non–dimensional variable
o	Reference scale or variable

Abbreviations

ADS	Automatic Depressurization System
BAF	Bottom of Active Fuel
DBA	Design–Basis Accident
BDLB	Bottom Drain Line Break
DPV	Depressurization Valve
DW	Drywell
h.t.c.	Heat Transfer Coefficient
GDCS	Gravity Driven Cooling System
GDLB	GDCS Line Break
H2TS	Hierarchical Two–Tier Scaling
IC	Isolation Condenser
ICS	Isolation Condenser System
LOCA	Loss–of–Coolant Accident
MIT	Massachusetts Institute of Technology
MSL	Main Steam Line
MSLB	Main Steam Line Break
NB	No–Break
NPP	Nuclear Power Plant
PCC	Passive Containment Cooler

PCCS	Passive Containment Cooling System
PIRT	Phenomena Identification and Ranking Table
PSI	Paul Scherrer Institute
RPV	Reactor Pressure Vessel
SBWR	Simplified Boiling Water Reactor
SC	Pressure Suppression Chamber
SP	Suppression Pool
SRV	Safety Relief Valve
TAF	Top of Active Fuel
UCB	University of California at Berkeley

ABSTRACT

This report presents a scaling study applicable to the SBWR–related tests. The scope of the study includes:

(a) a description of the scaling philosophy used for the GIST, GIRAFFE, PANDA, PANTHERS, and single–tube condensation–heat–transfer tests which have been, or will be, conducted in support of the SBWR program;

(b) the description of a set of scaling laws which are applicable to the SBWR–related test facilities; and

(c) an evaluation of the test facilities with respect to the proper scaling of the important phenomena and processes identified in the SBWR Phenomena Identification and Ranking Table (PIRT).

The study is fundamentally motivated by the need to demonstrate that the experimental observations from the test programs are representative of SBWR behavior. This includes an identification of any distortions in the representation of the phenomena and the manner in which these distortions can be considered when the experimental data are used for computer code qualification or the development of computer code models.

The Hierarchical Two–Tier Scaling (H2TS) methodology developed by the US NRC is applied to the extent practical throughout the study. Several scaling considerations addressed by H2TS are automatically satisfied in the SBWR–related experiments where, in all cases, the fluids and their thermodynamic states are prototypical. The various scaling issues are addressed, as appropriate, by either the top–down or bottom–up methodologies embodied in H2TS. The top–down scaling technique, as applied to generic *containment–related processes*, leads to a familiar set of scaling laws with a *system scale* for power, volume, horizontal area in volumes, and mass flow rate, and 1:1 scaling for pressure differences, elevations, and vent submergences.

The scaling of SBWR system components in relation to specific highly–ranked phenomena and processes is conducted according to the bottom–up H2TS methodology. This includes consideration of thermal plumes, mixing and stratification; heat and mass transfers at liquid–gas interfaces; the heat capacity of structures and heat losses; scaling of the vents; and heat and mass transfer in the condensers used for decay heat removal in the SBWR design. Finally, the scaling approach followed in designing the various SBWR–related facilities is reviewed in relation to the main purpose of the tests. The data collected from these facilities are used in the qualification of the system code TRACG.

1. Introduction

1.1 The SBWR and Related Tests

The SBWR uses gravity or natural circulation–driven, passive safety systems to provide emergency core coolant in case of a break in the primary system, to keep the core cooled and to remove decay heat from both the primary system and/or the containment. The main systems performing these tasks are the Gravity–Driven Cooling System (GDCS), the Isolation Condenser System (ICS), and the Passive Containment Cooling System (PCCS) (Vierow et al., 1992), Figure 1–1.

Emergency core cooling water is provided to the core by the GDCS. This system consists of three water pools situated above the top of the core, from which makeup coolant can flow by gravity to replenish the coolant lost from the Reactor Pressure Vessel (RPV). However, the GDCS can operate only after depressurization of the RPV; therefore, the SBWR is equipped with an Automatic Depressurization System (ADS) that performs this function. The depressurization of BWR primary systems is well understood, since it has been studied extensively in relation to the classical BWR designs. Indeed, the phenomena taking place during the early phase of blowdown inside the RPV have been extensively investigated by several series of tests; these constitute the basis for the corresponding qualification of the TRACG code (Andersen et al., 1993b). The containment loads during early blowdown have also been extensively investigated (GE, 1980; NRC, 1984; GE, 1987). The GDCS is, however, a relatively novel concept and requires some attention. The General Electric Company (GE) has therefore conducted the GDCS Integrated Systems Test (GIST) series of tests to investigate the behavior of the SBWR during the latter part of the depressurization phase. Proof of the technical feasibility of the GDCS concept was a major test objective.

Decay heat removal from the primary system while it is intact or under high pressure is performed by the ICS. The ICS consists of three Isolation Condensers (IC) located in a pool on top of the reactor building. When redundant squib valves are opened, steam from the primary system flows into the tubes of the ICs, condenses, and returns to the RPV, removing stored energy and is well understood, since such units have been in operation for many years in older BWRs. Thus, there is no specific need to experimentally verify the high–pressure operation of the SBWR decay heat removal system.

Decay heat is removed from the drywell (DW) by the PCCS, which employs three PCC condensers also located in interconnected IC pool compartments on top of the reactor building. The PCC condenser tubes are permanently connected to the DW. A

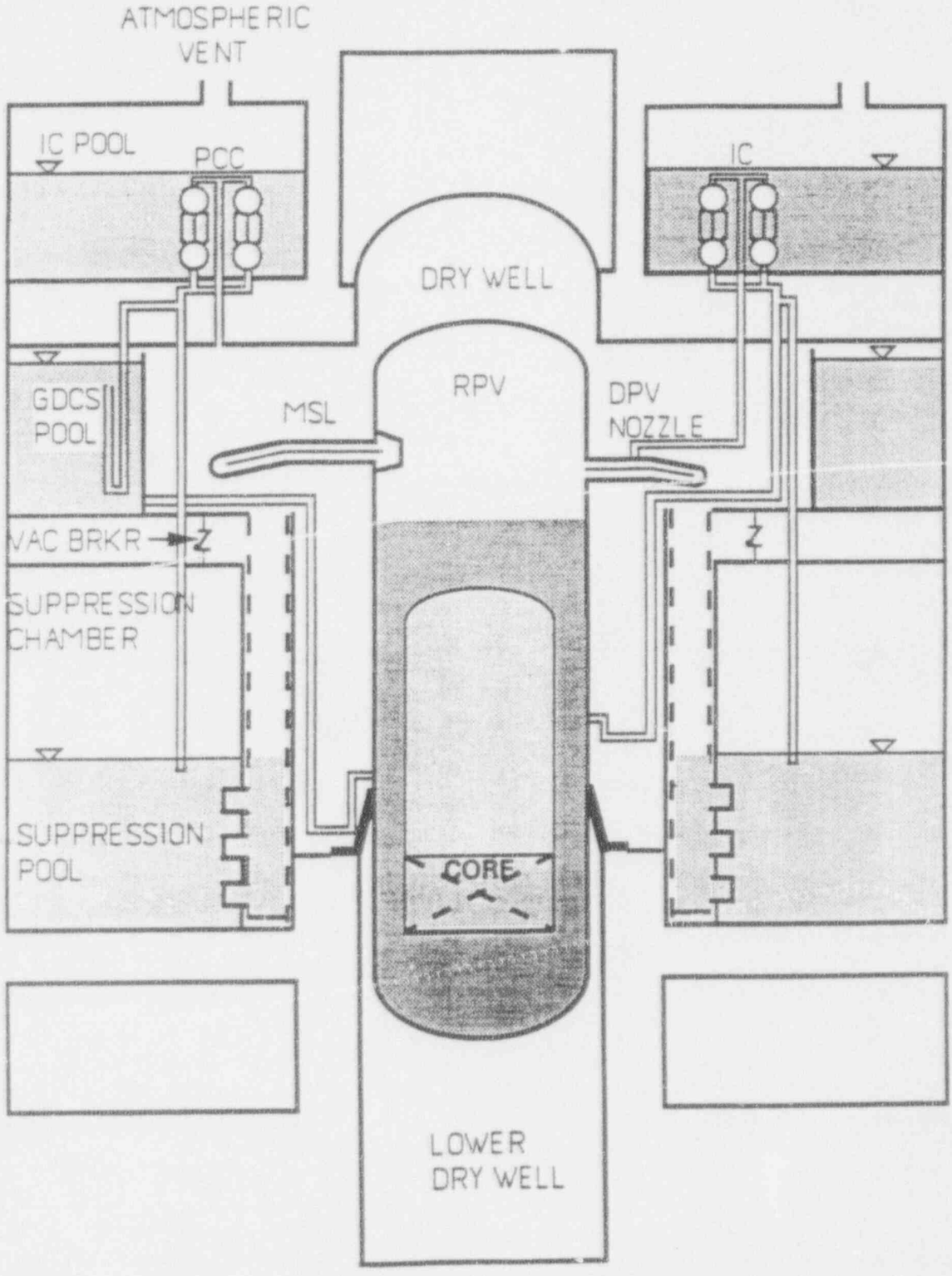

Figure 1–1 Passive Core and Containment Cooling Systems of the SBWR

mixture of steam and noncondensable gases (nitrogen present in the containment during normal operation) may enter the PCC condensers. The steam will condense, while the noncondensable gases must be vented to assure proper operation of the condensers. This is accomplished by conveying and venting the noncondensable gases into the suppression pool (SP) in the Suppression Chamber (SC) (or Wetwell).

Since the DW volume is connected directly to the SP either via the main pressure suppression vents or through the PCC condensers and their vent lines, the path that the steam will follow depends on the pressure differences between the DW volume and the two possible venting points. During the long-term containment cooling period, direct opening of the main vents and condensation of the steam in the SP must be avoided, since the SP is not provided with a safety-grade cooling system; the steam must be condensed in the PCC (or IC) condensers and any noncondensables vented to the SC. Although the operation of the condensers is understood, experimental verification of their integral, system behavior under a variety of conditions was deemed necessary. Two experimental facilities were provided for this purpose. The GIRAFFE facility, operated by Toshiba in Japan, provided extensive information about system behavior; this information was used to qualify the TRACG Code (Andersen et al., 1993a; Andersen et al., 1993b; Kim et al., 1993) for calculation of long-term decay heat removal and constitutes one of the major bases for certification of the SBWR (Vierow, 1993). The larger-scale PANDA facility, near completion at the Paul Scherrer Institute (PSI) in Switzerland, will provide additional information and will address issues such as the effects of the operation of several condenser units in parallel, the distribution of the constituents (steam and noncondensables) in the large DW volume, and mixing in the containment compartments. Availability of data from integral facilities having different scales is clearly an advantage for understanding system behavior and performing code qualification (Boucher et al, 1992). The PANDA experiments are part of the ALPHA program (Advanced LWR Passive Heat Removal and Aerosol Program) conducted at PSI.

The condensation of mixtures of steam and noncondensable gases in tubes under conditions expected in the PCC units has been investigated in experimental programs conducted at the Massachusetts Institute of Technology (MIT) (Siddique, 1992; Siddique et al., 1989, 1993) and at the University of California-Berkeley (UCB) (Vierow, 1990; Ogg, 1991; Vierow and Schrock, 1991). Full-scale tests of the IC and PCC units are being conducted at the PANTHERS facility at the SIET laboratory in Italy (Masoni et al., 1993).

Additional references about details of the various test facilities can be found in the letter by Marriott (1993). The design of all these experimental facilities and the conduct of the various tests was guided by consideration of the proper modeling and simulation of the various phenomena taking place. The objectives of this report are

to:

(1) summarize the philosophy used in defining the SBWR-related experimental program;

(2) describe the rationale used in scaling the various SBWR subsystems in the experimental facilities;

(3) verify the scaling criteria and laws used for the various facilities; and

(4) provide assurance that the phenomena of importance in relation to GDCS performance and long-term decay heat removal from the containment were properly addressed or represented in the tests.

1.2 General Approach for Code Qualification, Testing and Scaling

The approach adopted is similar to the one used for most LWR safety-related large-scale integral tests. It is clear that system tests (such as the GIST, GIRAFFE and PANDA tests) do *not* have to provide exact system simulations of the prototype. In fact, it is neither practical nor desirable to attempt to provide such exact simulations. However, system tests do provide *data* covering all essential phenomena and system behavior under a variety of conditions, which are used to qualify a system code (in the particular case, the TRACG Code used for safety analysis by GE).

To obtain data in the proper range of system conditions, the relative importance of the phenomena and processes present in the tests should not differ significantly from what is expected to take place in the SBWR. Similarly, the overall behavior of the test facility should not diverge significantly from that of the SBWR; in particular, one should not observe bifurcations in system behavior leading to quite different intermediate or end states. Finally, the tests should provide sufficiently detailed information, obtained under well-controlled conditions, to provide an adequate and sufficient database for qualifying the system code, TRACG.

Following current practice (INEL, 1989), a Phenomena Identification and Ranking Table (PIRT) was prepared for the SBWR post-LOCA containment phenomena. A PIRT identifies the phenomena and processes that are of particular importance during the various phases of a postulated accident or class of accidents. These phenomena receive, then, particular attention during code qualification. The SBWR PIRT was used to identify the phenomena of importance in relation to scaling of the experimental facilities. These phenomena are listed in Section 3 of this report (Table 3-1), where the scaling of specific phenomena is addressed.

1.3 Scope and Objectives of the Scaling Study

The scope of the scaling study reported here was to:

- Describe the scaling philosophy and strategy used in designing the various tests.
- Provide the applicable scaling laws.
- Show that the test facilities properly "scale" the important phenomena and processes identified in the SBWR PIRT and/or provide assurance that the experimental observations from the test programs are representative of SBWR behavior.
- Identify any distortions in phenomenology and/or scaling and discuss their importance; in particular, identify the ways by which such omissions and/or scaling distortions can be considered when the experimental data are used for code qualification.
- Verify the applicability of the condensation heat transfer data obtained in the single-tube university tests for the SBWR safety analysis.
- Provide the basis for showing that the experimental data are sufficient for qualifying TRACG.

1.3.1 Accidents and Accident Phases Considered

The range of accidents considered includes the main steam line break, as well as other breaks of the primary system, such as the GDCS line break and the bottom drain line break.

The scenario of these accidents can be rougly subdivided into three phases:

- The *blowdown phase* extending from the initiation of rapid depressurization by blowdown up to the time of refill of the LOCA vents. The blowdown phase can be further subdivided into an *early* phase extending until the time the pressure reaches a level of about 0.8 MPa, and a *late* blowdown phase thereafter.
- An intermediate *GDCS phase* during which the GDCS is delivering its stored water inventory to the primary system[a].
- A *long-term cooling phase* beginning when the GDCS inventory starts becoming replenished by the condensate flowing down from the ICS and PCCS (i.e., when the GDCS hydrostatic head necessary to drive flow into the core is made up by the ICS and PCCS condensate). At about the same time, the ICS and PCCS condensers become the dominant decay heat removal mechanism, replacing the heat sink provided by the water inventory initially stored in the GDCS pools.

The scaling analysis performed in this report is directed mainly at the scaling of reactor and containment components and phenomena which are significant over the time period starting with the latter blowdown phase and extending into the long–term cooling phase (see Section 1.3.1). As stated in the Introduction (Section 1.1), phenomena associated with the early stage of depressurization of a BWR vessel are well understood and are not considered to be part of the SBWR testing program. Thus, this report deals with *post–LOCA containment performance*.

1.3.2 Important Safety Issues

The tests conducted in relation to the SBWR are aimed at answering certain safety related issues, including:

- The possibility of core uncovery and damage — this issue is clearly related to the water inventory in the RPV resulting from the flows out of the break and from the GDCS, and to the RPV depressurization rate. This issue was addressed with the GIST tests, which demonstrated the feasibility of depressurizing the reactor core to sufficiently low pressures to enable reflooding by the gravity–driven flow from an elevated pool (Billig, 1989).
- Limitation of the containment pressure. This issue is related to the capability of the ICS and PCCS to remove decay heat. The distribution of phases in the various containment compartments and the temperature at the surface of the SP are significant variables.
- Effectiveness of condenation of steam injected into the SP from the PCCS vents.
- The performance of certain key containment components, such as: (1) the cyclic performance of the PCCS (in relation to venting of noncondensables), as observed in the GIRAFFE tests; (2) the intermittent opening of the vacuum breakers; and (3) the possible opening of the main vents during long–term containment cooling.
- The heat transfer performance of the ICS and PCCS condensers — this depends on both condensation heat transfer inside the condenser tubes in the presence of noncondensables and on heat transfer at the outside surface of the tubes in the pool, including IC pool inventory, temperature, and circulation rate. The possible degradation of the performance of the PCCS condensers due to insufficient venting and the accumulation of noncondensables in their tubes is also of importance.
- Structural integrity of the ICS and PCCS condenser units.

The issues identified above are addressed by the GIST, GIRAFFE, PANDA, and PANTHERS tests.

[8] For certain scenaria, GDCS flow may start before the end of the blowdown phase.

1.4 The H2TS Scaling Methodology

The NRC, in relation to Severe Accident Research, has developed a "structured" scaling methodology, which "provides the confidence that scaled experiments faithfully reproduce the phenomena which will occur in a NPP" (NRC, 1991). This methodology, referred to as Hierarchical, Two-Tiered Scaling (H2TS), addresses the scaling issues in two tiers: a top-down (inductive) system approach, followed by a bottom-up (deductive) process-and-phenomena approach. The method uses characteristic time ratios and a hierarchical characterization of the processes according to their temporal and spatial scales. To establish a hierarchical architecture for the system considered, one proceeds with a physical decomposition according to interacting subsystems, modules, constituents (materials), phases, and their geometrical configuration.

The H2TS methodology is applied to the extent necessary and practical in this work. Indeed, several scaling considerations that are addressed by H2TS are automatically satisfied in the SBWR-related experiments, in which the fluids and their thermodynamic states are prototypical (water and noncondensable gases under the pressures, temperatures, and concentrations expected in the SBWR). Moreover, the experiments are conducted at scales at which "microscopic" level interactions between phases (e.g., *local* mixing of gases) are not expected to be affected by the scale of the experiments. Thus, several hierarchical levels, related to constituents and phases, need not to be addressed.

1.5 Scaling Issues for the SBWR Related Tests

The experimental program supporting SBWR safety analysis includes the tests listed in Table 1-1, together with their volume scales in relation to the actual SBWR.

All these tests were (or will be) conducted under the following conditions:

- Actual fluids (water and steam, noncondensables, with the exception of substitution of air for nitrogen in most tests and of helium for hydrogen in all tests where hydrogen presence was simulated).
- Prototypical initial thermodynamic state of the fluids or mixtures (pressure, temperature, component concentrations).
- Full height.
- Test facilities are large enough (i.e., pipe and vessel dimensions have a sufficiently large characteristic length scale) so that "microscopic" level

Table 1-1

The SBWR Related Tests

Test	Purpose	Volume Scale
GIST	Integral GDCS system test	1/508
GIRAFFE PANDA	Integral long-term containment heat removal tests	1/400 1/25
PANTHERS	Structural and heat transfer tests of the ICS and PCCS condensers	Full-scale prototypes
UCB MIT	Condensation in the presence of noncondensables	Single-tube (near full-scale)

interactions between the phases (e.g., *local* mixing of two different gases) are not expected to be scale dependent.

The geometrical "macroscopic" level configuration of the phases needs to be considered, however, and leads to the requirement of preservation of the large-scale mixing behavior of fluids in single-phase situations, and of flow regimes in two-phase flow situations. The large-scale mixing issues are addressed in subsequent sections of this report. Scaling requirements to preserve flow regimes are discussed by Schwartzbeck and Kocamustafaogullari (1988). For the SBWR-related tests considered here, the geometrical scale of the models was sufficiently large so that important flow regime distortions are not expected; in addition, most containment flows are single-phase.

These considerations and design requirements remove any hierarchical concerns regarding constituents and phases, as mentioned above. Moreover, the full-height design of the experimental facilities leads to proper simulation of the natural gravity heads that are essential for the natural circulation systems and loops considered here. The remaining *geometrical* scaling issues are addressed in this report.

Additional scaling issues examined in this report include: (1) scaling of phenomena and processes; (2) multidimensionality, and (3) multi-unit, multi-element operation.

1.5.1 Scaling of Phenomena and Processes

The influence of spatial scale on phenomena and processes is considered in a bottom-up fashion for those ranked as important in the SBWR PIRT (e.g., stratification in pools and the development of thermal plumes).

1.5.2 Multidimensionality - Non Uniform Distribution Effects

This issue is related to the large differences in spatial scales between experiments like GIRAFFE and GIST and the SBWR. One must ensure that non-homogeneities in the distribution of constituents or phases that may be occurring at a particular scale are understood (and/or "scaled" properly whenever possible). The issue is addressed (Section 3.2) by running counterpart tests in facilities having different scales (GIRAFFE and PANDA) and by examining the physical reasons that may lead to such non-homogeneities in a phenomenological, bottom-up fashion.

1.5.3 Multi-Unit, Multi-Element Operation

The SBWR has multiple key components such as the ICS and PCCS condensers and vent lines. Moreover, the condensers have a large number of similar elements (tubes). The exact numbers of units, or elements per unit, cannot be duplicated in the experiments, and this raises the question of possible dissimilar, non-symmetric operation of the units or elements and its effects on system performance. Again the issue is addressed by analysis and by running tests in facilities having a range of number of tubes or units in parallel: (1) single-tube university tests; (2) three-tube GIRAFFE tests; (3) 20-tube, 4-unit PANDA tests; and (4) testing of entire full-scale modules in PANTHERS.

1.6 System Considered

1.6.1 Subdivision of the System into Subsystems and Components

For the purposes of this study, the SBWR System is subdivided into the subsystems or components shown on Table 1-2; their scaling by class of subsystem is considered in this report. Interactions (in this particular case, essentially transfers of mass and energy) between components are also a scaling consideration. The remaining SBWR systems or components are not relevant to this study and thus are not considered here.

Table 1-2

SBWR Subsystems and Components Considered

Reactor Pressure Vessel, RPV
Main Steam Lines (MSL) and Depressurization Valves (DPV)

Drywell, DW
- Upper DW volume
- DW annular volume surrounding RPV
- Lower DW volume below RPV skirt

Suppression Chamber, SC
- Gas space
- Liquid volume in suppression pool (SP)

Main (LOCA) vents connecting DW to SP (8)
Vacuum breakers between DW and SC (3)
Leakage path between DW and SC

Gravity-Driven Cooling System (GDCS) pools (3)
- Gas space
- Liquid space

Equalization line with check valve connecting SP to RPV (3)

Isolation Condenser System (ICS) condensers (3)
Passive Containment Cooling System (PCCS) condensers (3)
Noncondensable PCCS vent lines from condensers to SP (3)
Isolation Condenser Pool with interconnected subcompartments

Other lines connecting the various subsystems listed above.

1.6.2 Fluids and Other Materials

The *differences* between prototypical fluids and other materials that enter into consideration are:

- Air is used instead of nitrogen in the PANTHEI S, GIST, and PANDA system tests and in the UCB and MIT single-tube tests.
- Helium is used to simulate hydrogen in all related tests.
- The wall materials used in the SBWR and in the various integral facilities are different. This issue is discussed in Section 3.4, which deals with the heat capacity and conduction in containment structures.

2. General Scaling Considerations – Top–Down Approach

The SBWR and the corresponding scaled test facilities are referred to generically and collectively as the "System" or "SBWR System" in this report. Alternatively, the SBWR and a particular test facility are referred to, following common practice in scaling studies, as the "prototype" and the "model," respectively.

The *general* scaling criteria applicable to the SBWR System with its various subsystems and components and their counterparts in the related tests under consideration are derived in this section by a top–down approach. General scaling criteria have been derived by several authors (e.g. Ishii and Kataoka, 1983; Kocamustafaogullari and Ishii, 1984; Kiang, 1985; Boucher et al. 1991). Generally, these are not specific to the combined thermodynamic and thermal–hydraulic phenomena taking place inside containments and therefore are not directly applicable here. To arrive at general scaling criteria applicable to the SBWR System, the controlling processes in generic subsystems having the essential characteristics of *classes* of SBWR subsystems (e.g. containment volumes, pipes, etc.) are considered.

The SBWR System consists of a number of volumes (RPV, DW, SC, etc.) connected via junctions (i.e., openings, piping, vents, heat exchanging equipment — e.g., the ICS and PCCS condensers — fans, etc.). Mass and energy transfers take place between these volumes through their junctions. Heat may also be exchanged between volumes by conduction through the structures connecting them. These exchanges lead to changes in the thermodynamic condition of the various volumes; this, in particular leads to changes of the volume pressures. The junction flows (flows between volumes) are driven by the pressure differences *between* volumes. Thus, the *thermodynamic behavior* of the system (essentially, its *pressure history*) is linked to its *thermal–hydraulic behavior* (the flows of mass and energy between volumes). Proper scaling of these processes is the goal of the SBWR–related tests considered here and the topic addressed in this section.

The generic processes considered in this section are:

(1) The effects of the addition of heat and mass to a gas or liquid volume (namely, the resulting rates of change of the pressure).

(2) The rates of phase change at interfaces such as pool surfaces.

(3) Flows of mass between volumes.

Prototypical fluids under prototypical thermodynamic conditions were used in all the SBWR–related tests. The fact that the fluids are expected (by design and operation of the test facilities) to be in identical states in the prototype and the models, will

be used to simplify the following analyses.

For the top–down approach taken in this section, it is further assumed that the *composition* of the various fluids in different parts of the models (e.g., the fraction of noncondensables) remains also prototypical. The conditions that must be satisfied to ensure this additional requirement are examined in the following bottom–up study (Section 3), in which the particular phenomena affecting the *distribution* of the fluid composition are considered. One such example is stratification that may affect the composition of the fluids being transferred between volumes or the conditions at interfaces between liquid and gas volumes.

The first two processes listed above (1 and 2) confirm, as shown below, the validity of the (familiar) scaling of all the following variables with the "system scale" :

power : volume : horizontal areas in volumes : mass flow rate

A time scale of 1:1 between prototype and models has been adopted for all tests; however, this is not a necessity. Under certain conditions, the choice of a scale for the volumes different from the "system scale" will lead to accelerated (or decelerated) tests in time; this possibility is discussed in Section 2.4.4.

Process (3) will lead to the determination of the pressure drops and of the hydraulic characteristics of the junctions between volumes. In the SBWR System, certain pressure drops and the corresponding junction flows are controlled by the submergence depth of vents. The analyses of these processes will justify the choice of 1:1 scaling for the vertical heights in general and for the submergence depths in particular.

The pressure evolution resulting from the thermodynamics of the system and the pressure drops between volumes must clearly be scaled in an identical fashion. Considering the fact that prototypical fluids are used, this requirement links the properties of the fluid (in particular the latent heat and the specific volumes of water and steam) to the pressure differences between volumes (and to the submergence depths of vents), resulting in 1:1 scaling for pressure drops. Thus, the above considerations result in:

1:1 scaling for pressure differences, elevations, and submergences

This scaling rule determines the pipe diameters, lengths, and hydraulic resistances, and also determines the transit times between volumes. These transit times should, in principle, have the same (1:1) time scale as the inherent time constants of the system considered in the analysis of process (1). This matching cannot be perfect, but it is shown (Section 2.4.1) not to be important.

2.1 Thermodynamic Evolution of Containment Volumes with Mass and Energy Additions

Consider the control volume V of Figure 2–1 containing a mass M with internal energy E at a pressure p and a temperature T. The volume contains a number of constituents (noncondensable gases, steam, etc.) each denoted by the subscript j. Any changes in the kinetic and potential energy of the mass M are much smaller than changes in its intrinsic internal energy and therefore are neglected. The system is well mixed (i.e., the distributions of constituents and of the temperature are uniform, and at thermodynamic equilibrium).

The mass continuity equation for this volume is:

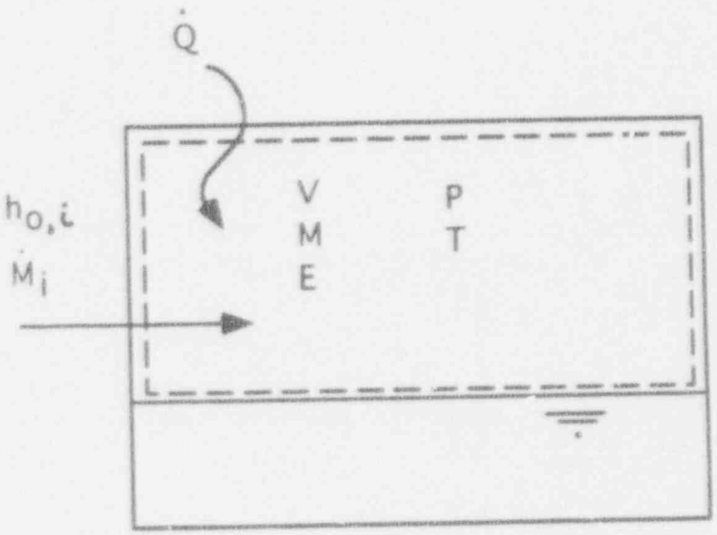

Figure 2–1 A Containment Volume (dashed line, in the case of a gas space) Receiving Mass Flow Rates $\dot{M}_i$ with Corresponding Total Enthalpies $h_{o,i}$, and Heat at the Rate $\dot{Q}$

$$\frac{dM}{dt} - \sum \dot{M}_i = 0 \tag{2.1}$$

where $\dot{M}_i$ are the mass flow rates entering the volume and carrying with them total enthalpy $h_{o,i}$. The total enthalpy (subscript o) includes the kinetic and potential energy of the various streams. The energy conservation equation is:

$$\frac{dE}{dt} = - p\frac{dV}{dt} + \dot{Q} + \sum \dot{M}_i h_{o,i} \tag{2.2}$$

where $\dot{Q}$ is the heat added to the system (e.g., by conduction through the wall). *Phase changes* taking place at interfaces bounding the control volume are considered, since these bring mass flow rates and enthalpies included in the $\sum \dot{M}_i$ and $\sum \dot{M}_i h_{o,i}$ terms.

The purpose here is to derive the equation relating the rate of change of the volume pressure dp/dt to the mass, enthalpy and heat additions (see, e.g., Section 2.14 of Moody, 1990). The specific internal energy of the system,

$$e = \frac{E}{M}$$

is a function of two thermodynamic variables, chosen here to be the pressure and the specific volume $v = V/M$, and of the mass fractions y_j of the various constituents:

$$e = e(p, v, y_j)$$

with

$$\sum y_j = 1$$

The differential of e can be calculated as:

$$de = \left.\frac{\partial e}{\partial p}\right|_{v,y_j} dp + \left.\frac{\partial e}{\partial v}\right|_{p,y_j} dv + \sum \left.\frac{\partial e}{\partial y_j}\right|_{p,v,y} dy_j \tag{2.3}$$

where the subscript y_j means that all y_j are kept constant, while the subscript y denotes that all y_j except the one appearing in the partial derivative are kept fixed. We note also that

$$E = Me \quad \text{and} \quad V = Mv$$

and therefore

$$\frac{dE}{dt} = \frac{d}{dt}(Me) = M\frac{de}{dt} + e\frac{dM}{dt} \tag{2.4}$$

$$\frac{dV}{dt} = M\frac{dv}{dt} + v\frac{dM}{dt} \tag{2.5}$$

Combining Equations 2.1 through 2.5:

$$\frac{dE}{dt} = M\left.\frac{\partial e}{\partial p}\right|_{v,y_j}\frac{dp}{dt} + M\left.\frac{\partial e}{\partial v}\right|_{p,y_j}\frac{dv}{dt} + M\sum\left.\frac{\partial e}{\partial y_j}\right|_{p,v,y}\frac{dy_j}{dt} + e\sum\dot{M}_i$$

$$= -pM\frac{dv}{dt} - pv\sum\dot{M}_i + \dot{Q} + \sum\dot{M}_i h_{o,i} \tag{2.6}$$

Solving this equation for dp/dt and using again Equations 2.5 and 2.1:

$$\frac{dp}{dt} = \frac{\sum\left[\dot{M}_i\left(h_{o,i} - e + v\left.\frac{\partial e}{\partial v}\right|_{p,y_j}\right)\right] + \dot{Q} - \left[p + \left.\frac{\partial e}{\partial v}\right|_{p,y_j}\right]\frac{dV}{dt} - \frac{V}{v}\sum\left[\left.\frac{\partial e}{\partial y_j}\right|_{p,v,y}\frac{dy_j}{dt}\right]}{\frac{V}{v}\left.\frac{\partial e}{\partial p}\right|_{v,y_j}} \tag{2.7}$$

We note that this equation yields the rate of change of the pressure in terms of the heat addition, of the mass and enthalpy fluxes into the volume, and the changes of volume composition. The rate of change of the volume dV/dt (e.g., due phase change) is also considered. The partial derivatives of e with respect to v, p and the mass fractions y_j, as well as their combinations with other thermodynamic variables, are *thermodynamic properties* of the particular mixture contained in the volume. Thus, the following short–hand notations for certain quantities appearing in Equation 2.7,

$$e^* \equiv e - v\left.\frac{\partial e}{\partial v}\right|_{p,y_j}$$

$$p^* \equiv p + \left.\frac{\partial e}{\partial v}\right|_{p,y_j}$$

$$f_{1,j} \equiv \frac{1}{v}\left.\frac{\partial e}{\partial y_j}\right|_{p,v,y} \quad \text{(units of energy per unit volume)}$$

$$f_2 \equiv \frac{1}{v} \left.\frac{\partial e}{\partial p}\right|_{v,y_j} \qquad \text{(non dimensional)} \tag{2.8}$$

denote thermodynamic properties of the mixture, which are functions of p, v, and the y_j. When prototypical fluids under prototypical thermodynamic conditions are used, these thermodynamic properties are identical for prototype and model.

The mass flow rates can be expressed as products of the volumetric flow rates $\dot{J}$ times the corresponding densities:

$$\dot{M}_i = \dot{J}_i \, \rho_i$$

Thus, Equation 2.7 takes the simpler form:

$$\frac{dp}{dt} = \frac{\sum \left[\dot{J}_i \rho_i (h_{o,i} - e^*)\right] + \dot{Q} - p^* \frac{dV}{dt} - V \sum \left[f_{1,j} \frac{dy_j}{dt}\right]}{V \, f_2} \tag{2.9}$$

The following reference quantities (denoted by the superscript ^{o}) are used:

- For volume: V^o
- For volumetric flow rates: $\dot{J}^o$
- For heat addition: $\dot{Q}^o$
- For densities: ρ^o
- For pressure, a reference pressure difference: Δp^o
- For enthalpies and internal energies, a reference enthalpy difference: Δh^o

A reference time is obtained by combining the volume and volumetric flow rate scales:

$$\tau^o = \frac{V^o}{\dot{J}^o} \tag{2.10}$$

This reference time τ^o is the *volume fill time* (or *residence time*) for mass flowing into the volume V^o at the volumetric flow rate $\dot{J}^o$ (Zuber, 1991).

Equation 2.9 will be non–dimensionalized by dividing the dimensional variables z by the reference values z^o above; this produces the non–dimensional variables z^+:

$$z^+ \equiv \frac{z}{z^o} \tag{2.11}$$

In particular, note that

$$e^* = e^{*+}\ \Delta h^o$$

$$p^* = p^{*+}\ \Delta p^o$$

$$f_{1,j} = f^+_{1,j}\ \Delta h^o\ \rho^o \tag{2.12}$$

The mass fractions y_j and f_2, being non–dimensional, require no scaling:

$$y_j = y_j^+ \qquad \text{and} \qquad f_2 = f_2^+$$

By non–dimensionalization, Equation 2.9 takes the form:

$$\frac{dp^+}{dt^+} = \frac{1}{f_2^+ V^+}\left[\ \Pi_{hp}\ \sum\left[\dot{J}_i^+ \rho_i^+ (h^+_{o,i} - e^{*+})\right] + \Pi_1\ \dot{Q}^+ - p^{*+}\ \frac{dV^+}{dt^+} - \Pi_{hp}\ \sum\left[f^+_{1,j}\ \frac{dy_j^+}{dt^+}\right]\ \right] \tag{2.13}$$

Two non–dimensional groups appear in the equation above:

$$\Pi_1 \equiv \frac{\dot{Q}^o\ \tau^o}{\Delta p^o\ V^o} \tag{2.14}$$

and

$$\Pi_{hp} \equiv \frac{\Delta h^o}{\Delta p^o/\rho^o} \tag{2.15}$$

Π_{hp} can be called the *enthalpy–pressure number* and links the enthalpy and pressure scales. It appears in front of the terms describing the effects of enthalpy additions and changes of composition in the volume and "converts" these effects into pressure changes.

Π_1 can be divided by Π_{hp} to yield a form of the familiar enthalpy or phase–change number (Yadigaroglu and Bergles, 1972; Saha et al. 1976)

$$\Pi_{pch} = \frac{\Pi_1}{\Pi_{hp}} \equiv \frac{\dot{Q}^o}{\dot{J}^o \rho^o \Delta h^o} = \frac{\dot{Q}^o}{\dot{M}^o \Delta h^o} \tag{2.16}$$

where $\dot{M}^o \equiv \dot{J}^o \rho^o$ is a reference mass flow rate. We will see later that the latent heat is a natural scale for the reference enthalpy difference. Thus, the phase change

number "converts" the heat additions into enthalpy differences.

The enthalpies h_o appearing in the energy conservation equations (Equations 2.2 or 2.9) are *total* enthalpies (i.e., the sum of the intrinsic enthalpy of the fluid plus its kinetic and potential energies). Consequently, the exact scaling of these would have required separate consideration of enthalpy, velocity, and elevation scales. Since changes in kinetic and potential energy are very small or totally negligible, this complication can be avoided.

2.1.1 Case of a Perfect Gas

To gain some physical understanding regarding f_2, e^* and p^*, consider the *case of a perfect gas*. The thermodynamic property f_2 scales the relative non–dimensional volume changes with pressure. For a perfect gas, $pv = RT$ and $R = c_p - c_v$, where c_p and c_v are the specifi. heats at constant pressure and volume, respectively, k their ratio, c_p/c_v, and R the perfect gas constant for the particular gas considered.

From the definition of c_v

$$e = c_v T = c_v \frac{RT}{R} = \frac{c_v}{c_p - c_v} pv = \frac{pv}{k - 1} \tag{2.17}$$

Thus

$$f_2 = \frac{\partial e/\partial p|_v}{v} = \frac{\frac{v}{k-1}}{v} = \frac{1}{k-1}$$

is in this case a constant. The property e^* becomes

$$e^* \equiv e - v \left.\frac{\partial e}{\partial v}\right|_p = e - v \frac{p}{k-1} = e - e = 0$$

We realize that e^* is not expected to attain very large values in real gas mixtures and $h_{o,i}$ should dominate the $(h_{o,i} - e^*)$ term. Thus, one sees that the first term on the right side of Equation 2.13 is not negligible and, to account properly for the effects of both enthalpy and heat additions to the system, *both* non–dimensional numbers appearing in Equation 2.13 (i.e., Π_{hp} and Π_1) or, alternatively, the more familiar set Π_{hp} and Π_{pch}, must be preserved.

Finally, for an ideal gas again, using Equation 2.17,

$$p^* = p + \left.\frac{\partial e}{\partial v}\right|_p = p + \frac{p}{k-1} = \frac{k}{k-1}\,p$$

From Equation 2.13 one notes that the effect of relative changes in volume is "amplified" by this ratio p^* to produce relative changes in pressure.

2.1.2 Specific Frequencies of the Process

Another way of viewing the processes taking place is by considering their specific frequencies and time constants (Zuber, 1991).

Specific frequencies are given as ratios of a transfer intensity to capacity (amount) of the receiving volume (Zuber, 1991). In the particular case considered here, two specific frequencies involved are the ratio of heat addition $\dot{Q}^o$ and enthalpy addition $\dot{M}^o\Delta h^o$ to the heat capacity of the receiving volume $V^o\rho^o\Delta h^o$:

$$\omega_{\dot{Q}} \equiv \frac{\dot{Q}^o}{V^o\rho^o\Delta h^o}$$

and

$$\omega_{\Delta h} \equiv \frac{\dot{M}^o\Delta h^o}{V^o\rho^o\Delta h^o}$$

A *residence* or *fill* time τ^o has already been defined,

$$\tau^o \equiv \frac{V^o}{j^o} \qquad (2.10)$$

The product of $\omega_{\dot{Q}}$ and τ^o results in the phase change number,

$$\omega_{\dot{Q}}\cdot\tau^o = \Pi_{pch}$$

as expected, while $\omega_{\Delta h}\cdot\tau^o = 1$; no new non–dimensional number is derived.

A third specific frequency is the ratio between the intensity of enthalpy addition $\dot{M}^o\Delta h^o$ and the "capacity of the volume to absorb work" $V^o\Delta p^o$:

$$\omega_{\Delta p} \equiv \frac{\dot{M}^o\Delta h^o}{V^o\Delta p^o}$$

The product of $\omega_{\Delta p}$ with τ^o produces, as expected, the enthalpy–pressure number

Π_{hp},

$$\omega_{\Delta p} \cdot \tau^{o} = \Pi_{hp}$$

In summary, the preceding analysis revealed the presence of two non dimensional numbers, Π_{hp} and Π_{pch} and a time scale for the system, τ^{o} (Equations 2.15, 2.16, and 2.10, respectively). Identical values for the non–dimensional numbers will have to be maintained in the prototype and the model.

2.2 Phase Changes at Interfaces

The phase changes at interfaces involve the latent heat of vaporization and the interfacial mass flow rates and mass fluxes. These are considered in this section.

2.2.1 Latent Heat of Vaporization

An arbitrary enthalpy reference scale Δh^{o} was used in the previous section. It is obvious that this arbitrary value could be chosen to coincide with the latent heat of the liquid used. Indeed, in systems with phase change, this seems to be the obvious choice. A simple confirmation of this fact will be provided here by considering mass continuity in a volume where phase change and mass transfers are taking place.

Figure 2–2 shows such a system consisting of the gas space with a mass M:

$$M = V \sum \rho_{j}$$

where ρ_{j} are the partial densities of the constituents. For simplicity, consider a saturated mass of liquid vaporized by a heater providing power at the rate $\dot{Q}$. A mass flow rate $\dot{M}_{ex}$ leaves the vapor space of the system. Mass continuity for the vapor space results in:

$$\frac{dM}{dt} = \dot{M}_{LG} - \dot{M}_{ex} \tag{2.18}$$

where $\dot{M}_{LG}$ is the mass transfer rate by boiling given by

$$\dot{M}_{LG} = \frac{\dot{Q}}{h_{fg}} \tag{2.19}$$

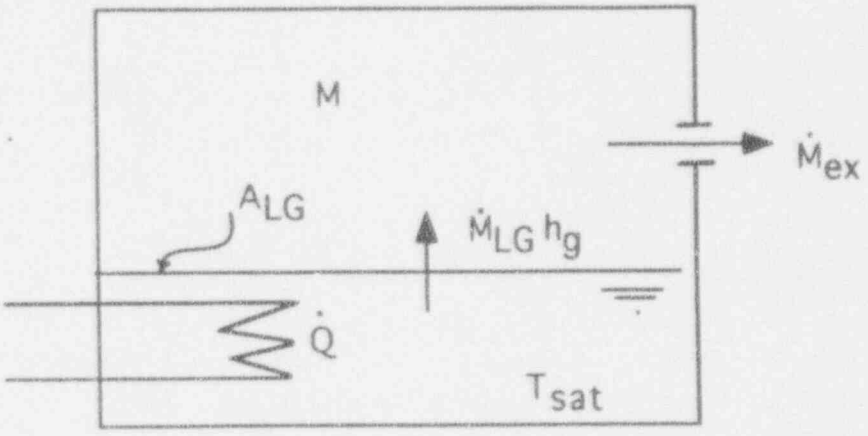

Figure 2–2 A volume containing a pool of boiling water.

where h_{fg} is the latent heat of vaporization. Combining Equations 2.18 and 2.19 and non–dimensionalizing using Q^o, V^o, j^o, ρ^o, and h_{fg}^o as scales, one obtains:

$$\frac{d}{dt^+}(V^+ \sum \rho_j^+) = \Pi'_{pch} \frac{\dot{Q}^+}{h_{fg}^+} - \dot{M}_{ex}^+ \tag{2.20}$$

We note that an alternative phase change number

$$\Pi'_{pch} \equiv \frac{\dot{Q}^o}{j^o \rho^o h_{fg}^o} \tag{2.21}$$

has appeared naturally. Comparing the two–phase change numbers Π_{pch} and Π'_{pch} (Equations 2.16 and 2.21, respectively), and considering their ratio, it becomes evident that we should have identical ratios of $h_{fg}^o/\Delta h^o$ in the prototype and the model. The scale of enthalpies Δh^o has not been specified so far; there is in principle no restriction for its choice. *When prototypical fluids under prototypical*

thermodynamic conditions are used in the model, it becomes evident that a natural way of satisfying the identical $h_{fg}^{o}/\Delta h^{o}$ ratio requirement[a] is to take:

$$\Delta h^{o} = h_{fg}^{o} \tag{2.22}$$

In other words the latent heat of the fluid provides a natural scale of enthalpies. Thus we also define

$$\Pi'_{hp} \equiv \frac{h_{fg}^{o}}{\Delta p^{o}/\rho^{o}} \tag{2.23}$$

This form of the enthalpy–pressure number will be used instead of Π_{hp} (Equation 2.15) in the following sections.

2.2.2 Rates of Phase Change

In the SBWR containment volumes, phase changes typically take place at the free surface of pools and on the walls. Condensation on structures and walls is limited by conduction within the structure and, therefore, depends strongly on the conduction characteristics of the walls. As already noted, conduction in the SBWR structures cannot easily be simulated by the experimental facilities (see Section 3.5 for details). It is left as an experimental parameter that must be addressed by measurement and detailed numerical calculations during data reduction.

In contrast, it is relatively straightforward to scale phase changes at the free pool surfaces. The flow rates due to phase change at the surface of a pool are given by the product of the pool surface area A_{LG} times the mass flux due to phase change $\dot{m}_{LG}$. The latter, in general, may depend on the fluid conditions on both sides of the interface (p, T, partial densities of constituents ρ_j) and on hydrodynamic parameters controlling mass transfer (i.e., the Reynolds and Prandtl numbers of the fluids). The hydrodynamic dependence is considered in the bottom–up analysis of Section 3. Here we derive the scaling of the surface areas. Since the phase change effects were included in the convective enthalpy terms of Equation 2.7, (by now separating these and showing them explicitly), we get, instead of the first term on the right side of Equation 2.13, two terms (the second term could also be a *sum* of terms involving phase change at several surfaces):

[a] It is not necessary to deal here with the more complex cases involving use of a different fluid or of the same fluid but at a different pressure level for the model, since neither of these alternatives was retained for any of the SBWR related tests. The choice of an alternative modeling fluid or of a non–prototypical pressure level leads to much more complex and restrictive scaling laws than the ones derived here.

$$\frac{dp^+}{dt^+} = \frac{1}{f_2 V^+}\left[\Pi'_{hp}\sum\left[j_i^+\rho_i^+(h_{o,i}^+ - e^{*+})\right] + \frac{\tau^o}{\Delta p^o}\frac{A_{LG}\dot{m}_{LG}^o h_{fg}^o}{V^o}\dot{m}_{LG}^+(h_g^+ - e^{*+})\right] + \ldots$$

We note a new non–dimensional number

$$\Pi_2 \equiv \frac{\tau^o}{\Delta p^o}\frac{A_{LG}\dot{m}_{LG}^o h_{fg}^o}{V^o}$$

Dividing Π_2 by Π'_{hp} (Equation 2.23), we find a second, *interfacial* phase change number:

$$\Pi_{ipch} \equiv \frac{\Pi_2}{\Pi'_{hp}} = \frac{A_{LG}\dot{m}_{LG}^o}{j^o\rho^o} \tag{2.24}$$

This number is the ratio of evaporative to convective mass addition. It can be used to scale the pool interfacial areas.

2.2.3 Specific Frequency for Phase Change

Again, we can define a specific frequency for phase change as the intensity of phase change (rate of vaporization) divided by the amount (capacity) in the receiving gas volume:

$$\omega_{vap} \equiv \frac{A_{LG}\dot{m}_{LG}^o}{V^o\rho^o}$$

Multiplying by the *fill* time of the process

$$\tau^o \equiv \frac{V^o}{j^o} \tag{2.10}$$

we obtain the interfacial phase change number:

$$\omega_{vap}\,\tau^o = \Pi_{ipch}$$

In summary, the analysis of this section has motivated the choice of a reference latent heat h_{fg}^o as *the* enthalpy scale to be used in the enthalpy–pressure and phase change numbers Π'_{hp} and Π'_{pch} (Equations 2.23 and 2.21) and yielded a new interfacial phase change number Π_{ipch} (Equation 2.24).

2.3 Transfers of Mass Between Volumes Driven by Pressure Differences

Mass transfers between containment volumes are driven by pressure differences; these could be due to differential pressure buildup in two different volumes or may also have hydrostatic causes. In this section, we derive the similarity laws governing such pressure–difference–driven mass flow rates in channels (pipes, ducts, etc) connecting various containment volumes.

The isolation condenser tubes constitute part of such piping in the SBWR. In all the SBWR–related tests, the isolation condenser tubes have prototypical dimensions and operate under prototypical flow and pressure drop conditions. Since pressure differences are generally also preserved in all tests, there are no scaling considerations for the pressure drop in the condenser tubes. Consequently, only the case of adiabatic channels is considered here. This, together with the assumption of incompressible flow made below, allows integration of the momentum equation assuming constant density and thus simplifies the analysis. Any heat exchanges between the fluid in channels connecting two volumes and the fluid within the volumes traversed are clearly small and are considered on an ad–hoc basis in both system calculations and for the experimental data reduction.

The general case (Figure 2–3) of a pipe connecting two volumes at pressures p_1 and p_2 is considered. In the receiving volume, the pipe may be immersed in a pool of liquid; in this case, we call it a *vent*. We consider here the case of an "open" vent with flow discharging from the vent.

The case of *single–phase flow* between the two volumes is treated here since this is the case in most pipes connecting SBWR volumes. The flow is treated as incompressible since, at the flow rates and pressure differences considered here, the vapor can be treated as such. (This question is analyzed in more detail in Section 2.4.2.) The analysis leads to the definition of the characteristics of the piping in the model.

For pipes that may carry *two–phase flow*, the analysis would be similar but would involve, in addition, a two–phase frictional multiplier, which is a function essentially of the fluid properties and of flow quality, and, to a much lesser extent, of the pipe diameter, flow rate and other secondary variables. Since the tests will be conducted with prototypical fluid conditions, the condition of the fluid entering the pipes will also be prototypical. For the adiabatic (or nearly adiabatic, except for heat losses) cases considered here, the two–phase multiplier will thus depend only on identical or very similar inlet conditions. The effects of the other variables mentioned above are expected to be of second–order importance. Thus, the analysis presented below applies also to piping carrying a two–phase mixture.

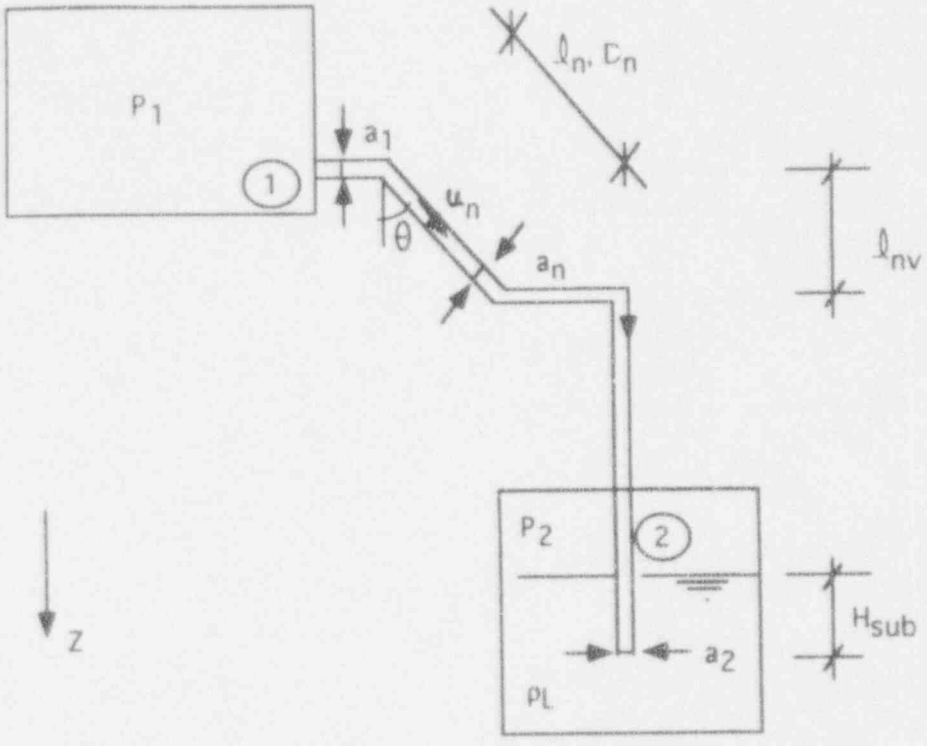

Figure 2–3 Pipe connecting two volumes and submerged in volume 2.

The one–dimensional momentum equation for time–dependent flow is:

$$\frac{\partial}{\partial t}(\rho u) + \frac{\partial}{\partial z}(\rho u^2) = - \frac{\partial p}{\partial z} + \rho g \cos\vartheta - \left[\frac{4f}{D} + k'_n \delta(z-z_n)\right]\frac{\rho u^2}{2}$$

The local losses at z_n are considered by the terms $k'_n\delta(z - z_n)$, where δ is the Kronecker delta. This equation is integrated between points 1 and 2 for the piping system of Figure 2–3, consisting of a number of segments (identified by the subscript n) having flow areas a_n and lengths l_n. The density ρ is taken as constant, as discussed above. The integration results in

$$(p_2 - p_1) = - \rho\left(\sum \frac{a_r}{a_n} l_n\right)\frac{du_r}{dt} - \rho\left(\frac{a_r^2}{a_2^2} - \frac{a_r^2}{a_1^2}\right)u_r^2$$

$$+ \sum \rho g l_{vn} - \frac{\rho u_r^2}{2} \sum F_n \left(\frac{a_r}{a_n}\right)^2 - \rho_L g H_{sub} \tag{2.25}$$

where

$$F_n \equiv \frac{4 f_n l_n}{D_n} + k_n \tag{2.26}$$

The k_n denote the local loss coefficients; the projections of the lengths of the various segments (having an angle of inclination ϑ) on the vertical axis are denoted by l_{vn}; H_{sub} is the submergence depth of the vent, and a_r is a reference cross section used to eliminate the u_n in favor of the reference velocity u_r. Indeed (for the case of constant–density flow considered here), from continuity:

$$a_n u_n = a_r u_r$$

The reference cross section a_r is related to the reference volumetric flow rate by

$$j^o = u_r^o a_r$$

The second term of Equation 2.25 has the same form as the F_n term and can be combined with it:

$$F \equiv \sum F_n \left(\frac{a_r^2}{a_n^2}\right) + 2\left(\frac{a_r^2}{a_2^2} - \frac{a_r^2}{a_1^2}\right) \tag{2.27}$$

The following parameters are also defined to simplify the notation:

The sum of the vertical projections of the various segments, L_g,

$$L_g \equiv \sum l_{vn} \tag{2.28}$$

and the equivalent *inertia* length of the piping, L_I,

$$L_I \equiv \sum \frac{a_r}{a_n} l_n \tag{2.29}$$

With these notations, Equation 2.25 takes the form

$$p_2 - p_1 = - \rho L_I \frac{du_r}{dt} + \rho g L_g - F \frac{\rho u_r^2}{2} - \rho_L g H_{sub} \tag{2.30}$$

Equation 2.30 is non–dimensionalized using as reference variables τ^o_{tp}, L_g, u^o_r, ρ^o, Δp^o, and H^o_{sub}, for times, velocities, densities, pressure differences, and submergence, respectively. Its non–dimensional form is:

$$(p_2^+ - p_1^+) = -\left(\frac{\rho^o L_l u_r^o}{\Delta p^o\ \tau_{tp}^o}\right) \rho^+ \frac{du_r^+}{dt^+} + \left(\frac{\rho^o g L_g}{\Delta p^o}\right) \rho^+ - \left(\frac{F\rho^o u_r^{o2}}{\Delta p^o}\right) \frac{\rho^+ u_r^{+2}}{2} - \left(\frac{\rho_L g H^o_{sub}}{\Delta p^o}\right) H^+_{sub} \tag{2.31}$$

Four non–dimensional numbers have appeared; they are all cast as ratios of the various pressures to the reference pressure drop. These are

The *inertial pressure drop number*

$$\Pi_{in} \equiv \frac{\rho^o L_l u_r^o / \tau_{tp}^o}{\Delta p^o} \tag{2.32}$$

a *hydrostatic pressure number*,

$$\Pi_{hyd} \equiv \frac{\rho^o g L_g}{\Delta p^o} \tag{2.33}$$

a *pressure loss* number,

$$\Pi_{loss} \equiv \frac{F\rho^o u_r^{o2}}{\Delta p^o} \tag{2.34}$$

and the *submergence pressure drop number*,

$$\Pi_{sub} \equiv \frac{\rho_L g H^o_{sub}}{\Delta p^o} \tag{2.35}$$

The reference pipe–transit time scale τ^o_{tp} can be chosen to be the *pipe inertial characteristic time*

$$\tau^o_{in} \equiv \frac{L_l}{u^o_r} \tag{2.36}$$

Then Π_{in} becomes

$$\Pi_{in} = \frac{\rho^o u_r^{o2}}{\Delta p^o} \tag{2.37}$$

Dividing Π_{hyd} by Π_{sub}, we get

$$\frac{\Pi_{hyd}}{\Pi_{sub}} = \frac{\rho^o}{\rho_L} \frac{L_g}{H^o_{sub}} \tag{2.38}$$

Since for prototypical fluids the density ratio ρ^o/ρ_L appearing in the equation above is preserved, we conclude that, instead of considering conservation of Π_{hyd}, it is sufficient to preserve the length ratio

$$\frac{L_g}{H^o_{sub}}$$

Finally, since

$$\Pi_{loss} = \Pi_{in} F$$

instead of Π_{loss}, it is sufficient to preserve Π_{in} *and* F or their product.

2.3.1 Transit Times in the Piping

We consider now the specific frequency of the transfers of mass in the piping. Again, considering the ratio of an intensity of transfer (the volumetric flow rate) to the (volumetric) capacity of the piping, we obtain

$$\omega_{tr} \equiv \frac{j^o}{\sum l_n a_n} = \frac{j^o}{L_V a_r} \tag{2.39}$$

where the equivalent volume–length of the piping L_V is

$$L_V \equiv \sum \frac{a_n}{a_r} l_n \tag{2.40}$$

The pipe transit time is the inverse of ω_{tr}:

$$\tau^o_{tr} \equiv \frac{L_V}{u^o_r} \tag{2.41}$$

The product of ω_{pt} times the inertial characteristic time τ^o_{in} (Equation 2.36) produces a non–dimensional number relating inertial and transit times:

$$\omega_{tr}\tau^o_{in} = \frac{\tau^o_{in}}{\tau_{tr}} = \frac{j^o}{L_V a_r}\frac{L_I}{u^o_r}$$

Since

$$j^o = a_r u^o_r$$

we find that

$$\omega_{tr}\tau^o_{in} = \frac{\tau^o_{in}}{\tau_{tr}} = \frac{L_I}{L_V}$$

Note that this ratio is equal to

$$\frac{L_I}{L_V} = \frac{\sum \frac{a_r}{a_n} l_n}{\sum \frac{a_n}{a_r} l_n} \qquad (2.42)$$

This produces another geometrical ratio that should be preserved.

In summary, the analysis of this section shows that we are left with L_g/H^o_{sub}, F (Equation 2.27) or the product $\Pi_{in}F$), the ratio L_I/L_V (Equation 2.42), and only Π_{in} and Π_{sub} (Equations 2.37 and 2.35, respectively), as the non–dimensional quantities to match between prototype and experiment. Two additional time scales τ^o_{in} and τ^o_{tr}, Equations 2.36 and 2.41, were also identified.

2.4 General Scaling Criteria

The criteria derived in Sections 2.1, 2.2, and 2.3 will be combined now to arrive at general scaling laws for the models of the SBWR.

Recall that the test facilities are designed to operate with prototypical fluids under prototypical thermodynamic conditions. In addition, the following **non–dimensional numbers** must be matched:

Enthalpy–Pressure Number

$$\Pi'_{hp} \equiv \frac{h^o_{fg}}{\Delta p^o/\rho^o} \tag{2.23}$$

Phase–Change Number

$$\Pi'_{pch} \equiv \frac{\dot{Q}^o}{\dot{j}^o \rho^o h^o_{fg}} = \frac{\dot{Q}^o}{\dot{M}^o h^o_{fg}} \tag{2.21}$$

Interfacial Phase Change Number

$$\Pi_{ipch} \equiv \frac{A_{LG}\dot{m}^o_{LG}}{\dot{j}^o \rho^o} = \Pi'_{pch}\,\frac{A_{LG}\dot{m}^o_{LG}h^o_{fg}}{\dot{Q}^o} \tag{2.24}$$

Inertial Pressure Drop Number

$$\Pi_{in} \equiv \frac{\rho^o u^{o2}_r}{\Delta p^o} \tag{2.37}$$

Submergence Number

$$\Pi_{sub} \equiv \frac{\rho_L g H^o_{sub}}{\Delta p^o} \tag{2.35}$$

In addition, we have defined three **time scales** that must be matched, namely τ^o, τ^o_{in}, and τ^o_{tr}:

$$\tau^o = \frac{V^o}{\dot{j}^o} \tag{2.10}$$

$$\tau^o_{in} \equiv \frac{L_l}{u^o_r} \tag{2.36}$$

$$\tau^o_{tr} \equiv \frac{L_V}{u^o_r} \tag{2.41}$$

and three **geometric parameters**,

$$\frac{L_g}{H^o_{sub}}$$

with L_g, the sum of the vertical projections of the piping segments defined by Equation 2.28; the ratio of the equivalent inertia and volume lenghts of the piping,

$$\frac{L_I}{L_V} = \frac{\sum \frac{a_r}{a_n} l_n}{\sum \frac{a_n}{a_r} l_n} \tag{2.42}$$

and the total flow resistance of the piping,

$$F \equiv \sum F_n \left(\frac{a_r^2}{a_n^2}\right) + 2\left(\frac{a_r^2}{a_2^2} - \frac{a_r^2}{a_1^2}\right) \tag{2.27}$$

where

$$F_n \equiv \frac{4 f_n l_n}{D_n} + k_n \tag{2.26}$$

As noted in Section 2.3, instead of preserving both F *and* Π_{in}, it is sufficient to preserve their product, Π_{loss} (Equation 2.34).

2.4.1 Comparison of the Time Scales

The three time scales produced by the analysis of the previous sections (τ^o, τ^o_{in}, and τ^o_{tr}) scale the rates of volume fill, of inertial effects, and of pipe transfers, respectively. Clearly, the systems considered here are made of large volumes connected by piping of much lesser volumetric capacity. The pressure drops between these volumes are not expected to be dominated by inertial effects. Thus the inertia and transit times, which are of the same order of magnitude, are much smaller than the volume fill times:

$$\tau^o >> \tau^o_{in} \approx \tau^o_{tr}$$

We conclude that the time scale that "must" be preserved is τ^o and we write

$$\tau_R = 1 \tag{2.43}$$

where the subscript R denotes the ratio between the corresponding scales of prototype and model for the variable z:

$$z_R \equiv \frac{z_{prot}}{z_{mod}}$$

The other two time scales (controlled by the geometric characteristics L_l and L_V of the piping) are clearly of lesser importance.

In other words, we expect the time behavior of the system to be controlled by the volume fill rates (or τ^o). The pipe transit times and the inertial time scale of the piping (τ^o_{tr} and τ^o_{in}) are much shorter; the overall dynamics of the system are not controlled by such effects. Thus, in relation to the time constants of the system, *the lengths of piping connecting containment volumes and the velocities in these pipes do not have to be scaled exactly.*

2.4.2 Compressibility of the Gas Flowing in Pipes

The gases flowing in pipes connecting containment volumes were treated as incompressible; this assumption is justified in this section.

We start from the continuity equation, written for the pipe segment of Figure 2–4,

$$\frac{dM}{dt} = \dot{M}_1 - \dot{M}_2 \qquad (2.44)$$

where $\dot{M}_1$ and $\dot{M}_2$ are the mass flow rates at Sections 1 and 2, respectively; in general

$$\dot{M} = A_p \rho u$$

M is the mass contained in the pipe of volume $V_p = A_p L_p$ and average density $\bar{\rho}$. We non–dimensionalize Equation 2.44 by defining

$$\dot{M}^+ \equiv \frac{\dot{M}}{\dot{M}^o_1}$$

$$\rho^+ \equiv \frac{\rho}{\rho^o_1}$$

and a pipe transit time

$$\tau^o_{tr} \equiv \frac{L_p}{u^o_1}$$

Equation 2.44 takes the non–dimensional form

$$\tau^{o}_{tr} \frac{d}{dt}\overline{\rho^{+}} = \dot{M}^{+}_{1} - \dot{M}^{+}_{2} \tag{2.45}$$

It is evident that if τ^{o}_{tr} and the rate of change of the average density are both small, the mass flow rates at the inlet and the exit of the pipe will be approximately equal, $\dot{M}^{+}_{1} \approx \dot{M}^{+}_{2}$, or $\dot{M}_{1} \approx \dot{M}_{2}$. Clearly, the pipe transit time τ^{o}_{tr} must be compared to the other time constants of the system; namely, the ones determining the variation of the conditions in the containment volumes (i.e., τ^{o}). The same volume fill constant τ^{o} determines the rate of variation of the inlet density ρ_{1} and, consequently, of the average density $\overline{\rho}$ in the pipe.

2.4.3 Length Scales of the System

The three geometric parameters that have appeared (i.e., L_{g}/H^{o}_{sub}, L_{l}/L_{v} and F) are considered now.

In facilities preserving vertical heights, the ratio L_{g}/H^{o}_{sub} is clearly conserved. The ratio L_{l}/L_{v} scaling inertial to transit times in the piping should not be very important, according to the discussion of Section 2.4.1. It can, however, approximately at least, be conserved. Thus, we require:

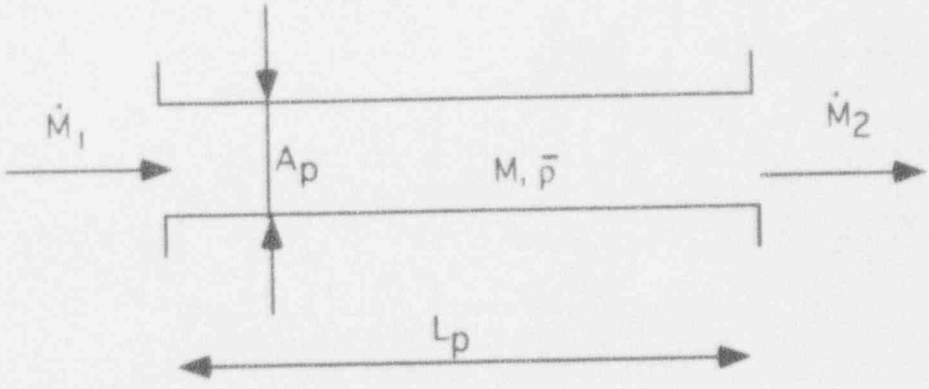

Figure 2–4 A pipe segment connecting two volumes.

$$\left(\frac{L_g}{H_{sub}}\right)_R = \left(\frac{L_l}{L_V}\right)_R = 1 \tag{2.46}$$

The factor F, (Equation 2.27) determining the total flow resistance of the piping is important. This factor does not have to be scaled alone, however, but rather as the product $\Pi_{in}F$, as shown in Section 2.3. The scaling of the pressure losses in the piping is considered in Section 2.4.5 below. Since the F values of the models can in general be larger than those of the prototypes (because of the smaller diameters in the ratio *fl*/D), the velocities in the model may end up being smaller than those of the prototype. This is not important as long as the transit times between volumes are small compared to the volume fill times τ^o, as discussed in Section 2.4.1.

2.4.4 Other Reference Scales in the System

We have already dealt with the time and geometric scales in the preceding two paragraphs. We can consider now the remaining five non–dimensional numbers listed at the beginning of Section 2.4 and repeated here for convenience:

Enthalpy–Pressure Number $$\Pi'_{hp} \equiv \frac{h^o_{fg}}{\Delta p^o/\rho^o} \tag{2.23}$$

Phase–Change Number $$\Pi'_{pch} \equiv \frac{\dot{Q}^o}{j^o \rho^o h^o_{fg}} \tag{2.21}$$

Interfacial Phase Change Number $$\Pi_{ipch} \equiv \frac{A_{LG}\dot{m}^o_{LG}}{j^o \rho^o} \tag{2.24}$$

Inertial Pressure Drop Number $$\Pi_{in} \equiv \frac{\rho^o u_f^{o2}}{\Delta p^o} \tag{2.37}$$

Submergence Number $$\Pi_{sub} \equiv \frac{\rho_L g H^o_{sub}}{\Delta p^o} \tag{2.35}$$

and the time scale τ^o,

$$\tau^o = \frac{V^o}{j^o} \tag{2.10}$$

To achieve proper scaling, the five non–dimensional numbers listed above must have the *same values for each pair of system and model components* (the values that a

non–dimensional number takes will of course vary between pairs of components). This leads to the definition of the proper scaling ratios between prototype and model. For example, conservation of the enthalpy–pressure number everywhere in the system leads to the scaling requirement:

$$\left(\frac{h_{fg}^{o}}{\Delta p^{o}/\rho^{o}}\right)_{R} = 1$$

for all system components[b].

The minimum set of independent reference scales appearing in the non–dimensional numbers listed above is:

$$h_{fg}^{o},\ \Delta p^{o},\ \rho^{o},\ \dot{Q}^{o},\ j^{o},\ A_{LG},\ \dot{m}_{LG}^{o},\ u_{r}^{o},\ \rho_{L},\ H_{sub}^{o},\ \text{and}\ V^{o}$$

The reference scales can be chosen uniquely for the entire system or, alternatively, for each system component. This does not make any difference, since it is only ratios of scales that must be compared between prototype and model; these ratios are the ones denoted by the subscript R, as shown below.

When prototypical fluids are used, h_{fg}^{o}, ρ^{o}, ρ_{L}, and $\dot{m}_{LG}^{o}$ need not to be considered. (Some reservations were already made regarding the conservation of the phase change flux $\dot{m}_{LG}^{o}$ in Section 2.2.2; these are discussed in Section 3.) Thus, we are left with only

$$\Delta p^{o},\ \dot{Q}^{o},\ j^{o},\ A_{LG},\ u_{r}^{o},\ H_{sub}^{o},\ \text{and}\ \ V^{o}$$

We are left with seven independent scales and only five non–dimensional numbers, plus an arbitrary "system scale" to be determined. However, no choice for a Δp^{o} scale has been made up to this point. The submergence hydrostatic head $\rho_{L} g H_{sub}^{o}$ is an important parameter, since it largely controls the flows of mass and energy between the SBWR containment volumes. Thus it appears to be the natural choice for the (so far, arbitrary) value of Δp^{o}. By dictating the use of the submergence hydrostatic head as *the* reference pressure drop, the submergence number Π_{sub} (Equation 2.35) takes the value:

$$\Pi_{sub} = 1$$

[b] The subscript R, already defined in Section 2.4.1, denotes the ratio between corresponding quantities in the prototype and the model.

in both prototype and model, and

$$\Delta p^{o} = \rho_{L} g H^{o}_{sub} \tag{2.47}$$

Thus, all pressure drops will scale with $\rho_{L} g H^{o}_{sub}$, and the submergence number Π_{sub} needs no longer to be considered. Insertion of Equation 2.47 in the enthalpy–pressure number, Equation 2.23, yields:

$$\Pi'_{hp} = \frac{\rho^{o}}{\rho_{L}} \frac{h^{o}_{fg}}{g H^{o}_{sub}} \tag{2.48}$$

Since the fluid is prototypical, $(\rho^{o} h^{o}_{fg}/\rho_{L})_{R} = 1$, and Equation 2.48 shows that the *submergence depths must be conserved* at a scale of 1:1,

$$(H_{sub})_{R} = 1 \tag{2.49}$$

Otherwise, the rates of pressure change due to thermodynamic evolutions (considered in Section 2.1) will not match the pressure differences driving the mass and energy transfers between volumes (considered in Section 2.3).

We are left now with five scales:

$$\dot{Q}^{o},\ \dot{j}^{o},\ A_{LG},\ u^{o}_{r},\ \text{and}\ \ V^{o}$$

and three non–dimensional numbers:

$$\Pi'_{pch},\ \Pi_{ipch},\ \text{and}\ \Pi_{in}$$

Conservation of the phase change number Π'_{pch} dictates the need to preserve the ratio $\dot{Q}^{o}/\dot{j}^{o}$. Similarly, conservation of the interfacial phase change number, Π_{ipch}, requires preservation of the ratio $A_{LG}/\dot{j}^{o}$. Clearly, this can only be achieved by

$$\dot{Q}_{R} = \dot{j}_{R}\ (= \dot{M}_{R}) = (A_{LG})_{R} = R \tag{2.50}$$

where R is the "system scale". Thus, heat addition, flow rates, and horizontal areas must scale with the system scale R. Since the volume scale V^{o} appears only in the time constant τ^{o}, one could in principle conduct tests at a different time scale (not 1:1) by modifying the volume scale V_{R}. This is possible as long as τ^{o} is *the* controlling time scale, as already discussed in Section 2.4.1. Accelerated tests can, for instance, be conducted by decreasing V_{R} or increasing equally the other scales, $\dot{Q}_{R} = \dot{M}_{R} = \dot{j}_{R} = (A_{LG})_{R}$. Conservation of the time scale τ^{o} also implies (in any

case) preservation of the ratio V^o/j^o.

2.4.5 Scaling of the Piping

Scaling of the pressure drops between compartments requires consideration of the product $F\Pi_{in}$, as shown in Section 2.3. Since $\Delta p_R = (\rho_L g H_{sub})_R = 1$, this amounts to

$$\left(u_r^2 F\right)_R = 1$$

Since

$$u_r^o = \frac{j^o}{a_r}$$

we obtain

$$\left(a_r^2\right)_R = \left(Fj^2\right)_R$$

or

$$(a_r)_R = \left(F^{\frac{1}{2}}\, j\right)_R \qquad (2.51)$$

This equation determines the reference flow area scale $(a_r)_R$. The factor F, Equations 2.26 and 2.27, depends on both the frictional losses in the pipes, i.e. on the groups $4f_n l_n/D_n$, and on the form losses k_n. The latter are generally insensitive to scale. Since the model diameters D_n are smaller, however, the F factors of the models tend to be larger. Thus Equation 2.51 leads to an increase of the model pipe diameters; this reduces the flow velocities.

In practice, pipe scaling is performed according to the following procedure: the pipe cross–sectional areas in the scaled facilities are oversized for convenience; this leads to somewhat lower flow velocities in the pipes. Thus, considering only the *form losses* (for which the loss coefficients are only weakly dependent on flow velocity or Reynolds number), the total Δp's in the models would be *lower* than prototypical. On the contrary, *wall friction* in the scaled facilities is *larger* (due to larger values of the f*l*/D values produced by the smaller pipe diameters), as it cannot be compensated in general by the decrease in velocity. Usually (and fortunately), the total pressure drops in the piping are dominated by form losses, so that the total Δp's in the scaled facilities end up being somewhat smaller. They can therefore be matched by introducing additional form losses by local orificing.

The pipe flow areas determined in this fashion result in velocities that do not lead to matching **pipe transit times**, as expected. Indeed, using Equation 2.51, the velocity scaling ratios are given as:

$$(u_r)_R = \left(\frac{j}{a_r}\right)_R = (F^{-\frac{1}{2}})_R \qquad (2.52)$$

As already noted, since the F values of the models are in general larger than those of the prototypes, the velocities in the model are generally smaller than in the prototype. This is not important as long as the transit times between volumes, τ^o_{tr} (Equation 2.41) are small compared to the volume fill times τ^o, as discussed in Section 2.4.1, and as long as extremely low velocities do not introduce new phenomena in the models.

The matching of the pressure drops in the various facilities is again discussed in Section 4: in summary, *matching of the total pressure drops is accomplished by using orifices in conjunction with convenient choices for pipe diameters.*

2.5 Summary

The analysis presented in this section has shown that, when prototypical fluids under prototypical thermodynamic conditions are used:

- The elevations in the prototype and in the model must be identical, especially the submergence depths of the vents.
- The volumetric flow rates, heat inputs and horizontal pool areas must be scaled according to the system scale R,

$$\dot{Q}_R = \dot{J}_R \ (= \dot{M}_R) = (A_{LG})_R = R \qquad (2.50)$$

- If, in addition, the volumes are also scaled with R,

$$V_R = R$$

the time scale between model and prototype is 1:1. In this case, we can speak of a vertical *slice* or vertical *section* model of the prototype.

- The pipe flow areas must be geometrically similar and the reference cross–sectional areas a_r must scale like

$$(a_r)_R = (F^{\frac{1}{2}}\ \dot{J})_R \qquad (2.51)$$

where the factor F, determining the total pipe losses, can be adjusted by introducing local losses in the model to match the pressure drops, if necessary.

– The pipe flow areas determined in this fashion result in velocities that do not match the pipe transit times; usually, the velocities in the model may be smaller than those of the prototype. This is, however, not important as long as the transit times between volumes are small compared to the volume fill times τ^{o}.

3. Scaling of Specific Phenomena – Bottom–Up Approach

The scaling of particular SBWR system components in relation to specific phenomena and processes considered important is conducted in a bottom–up fashion in this section. The discussion is limited to the spatial–scale–dependent phenomena ranked as important in the SBWR PIRT and not considered generically in Section 2.

3.1 Important Phenomena

The SBWR PIRT was used to identify the phenomena of safety importance for post–LOCA behavior of the SBWR. The important phenomena for each subsystem or component and for each phase of the class of accidents considered were identified. Table 3–1 lists all phenomena that received importance grades of 7, 8, or 9 on a scale of 0 to 9. The phenomena (in each of the three main phases of the class of accidents considered) are listed, together with the subsystems where they are expected to be of importance.

The last column of Table 3–1 shows how the scaling issue for each phenomenon was addressed. In several cases (e.g., "friction"), the scaling concern was addressed generically in the top–down scaling analysis of Section 2. Such phenomena are marked "top–down." In the case of condensation phenomena within the condenser tubes, scaling is addressed by the use of full–size tubes in system test facilities, supported by the single–tube tests at MIT and UCB. The University tests are summarized in Section 3.6.2. Detailed "bottom–up" scaling is provided in the following sections for the remaining phenomena identified in Table 3–1. In these cases the number of the particular section where the scaling is addressed is shown in the last column of the table.

3.2 Thermal Plumes, Mixing, and Stratification

Thermal plumes, mixing and thermal stratification phenomena can be encountered:

- In the DW and in the gas space of the SC, for steam and noncondensable gases (nitrogen or hydrogen).
- In the suppression pool.

Combinations of single–phase/two–phase, axisymmetric/plane, and free/wall plumes

Table 3–1
Important Phenomena Identified in PIRT

PHENOMENA/PROCESSES	LOCATION IN SYSTEM	SCALING
Late Blowdown Phase (of importance for GIST tests)		
Critical flow	break, main vents, SRV quenchers, DPV	top–down[a]
Friction	break, main vents, SRV quenchers, DPV, IC/PCC lines	top–down
Void fraction/interfacial shear	main vents, SRV quenchers, DPV	top–down
Phase separation/interfacial shear	DW, SC(SP)	top–down/Sec. 3.2
Liquid entrainment	break, main vents, SRV quenchers, DPV	top–down
Entrainment in jets	SC (SP: gas/liquid)	Sec. 3.5
Component separation/mixing	DW (gases)	Sec. 3.2.3
Flashing/evaporation	DW	top–down
Interfacial heat transfer/condensation	DW, SC(main + PCC vents, SRV quencher)	top–down/Sec. 3.5.2
Degradation of condensation	SC(gas space), SC(main + PCC vents)	top–down/Sec. 3.5.2
Condensation in tubes	IC, PCC	Univ. tests/Sec. 3.6.1
Degradation of condensation in tubes	PCC	Univ. tests/Sec. 3.6.1
Shear–enhanced condensation	IC tubes, PCC tubes	Univ. tests/Sec. 3.6.1
GDCS Phase (of importance for GIST, GIRAFFE, and PANDA tests)		
Friction	GDCS injection line	top–down
Condensation in tubes	IC, PCC	Univ. tests/Sec. 3.6.1
Degradation of condensation in tubes	PCC	Univ. tests/Sec. 3.6.1
Shear–enhanced condensation	IC tubes, PCC tubes	Univ. tests/Sec. 3.6.1
Long–Term Cooling Phase (of importance for GIRAFFE and PANDA tests)		
friction	PCC lines	top–down
Phase separation/interfacial shear	SC(gas space)	top–down, Section 3.2.2
Component separation/mixing	DW, SC(gas space)	Sec. 3.2.3
Mixing/entrainment into jets	DW (gases), SC(SP: gas/liquid)	Sec. 3.2, 3.5
Buoyancy/natural circulation	DW, SC(SP), IC pools	Sec. 3.2, 3.6.2
Forced flow	PCC fan	top–down
Interfacial heat transfer/condensation	SC, PCC vents, pool surfaces, containment spray	Sec. 3.3, 3.5.2
Degradation of condensation (n/c's)	SC, PCC vents, pool surfaces, containment spray	Sec. 3.3, 3.5.2
Condensation in tubes	PCC	Univ.tests/Sec. 3.6.1
Degradation condensation in tubes	PCC	Univ.tests/Sec. 3.6.1
Shear enhanced condensation	PCC tubes	Univ.tests/Sec. 3.6.1
Lateral entrainment in 2–phase flow	condensers in IC pool	Sec. 3.6.2
Component separation	PCC tubes	Univ. tests
Conduction in walls/int'nal structures	DW, SC	Not scaled/Sec. 3.4
Steam bypass/leakage	DW–SC	Top–down

[a] reduced to correct definition of the choked area

for fluids emerging from vents or originating on hot or cold wall surfaces can be encountered. The various stratification, plume, and jet situations are sketched in Figure 3–1.

The situations involving mixing induced by plumes are discussed in this section, while the condensation phenomena from either jets or two–phase plumes are considered in Section 3.5.2.

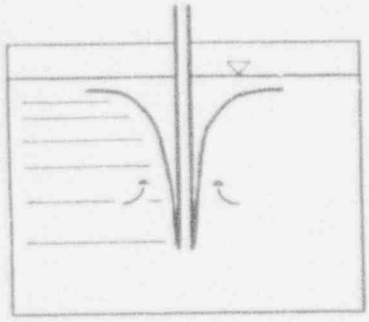

a) PCC vent into SP 1-phase

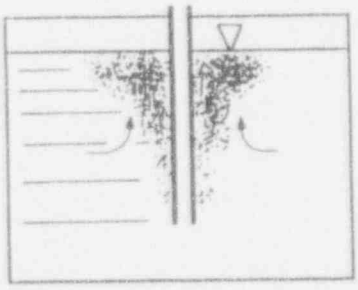

b) PCC vent into SP, 2-phase

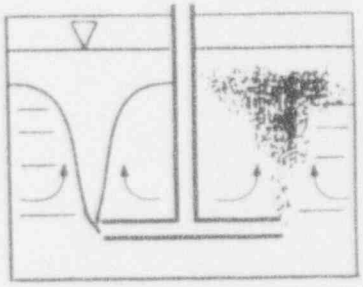

c) PCC vent into SP, 1- or 2-phase

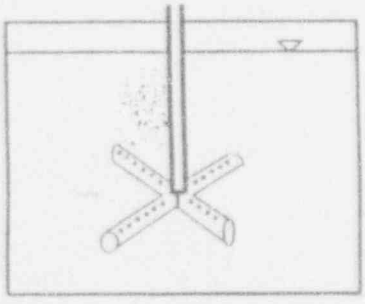

d) PCC vent with quencher ("linear source")

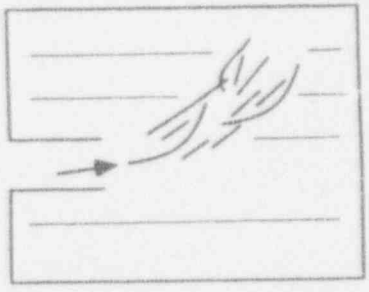

e) Steam injection into DW

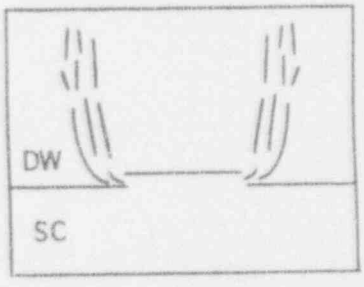

f) Vacuum breaker (circular ring linear source)

Figure 3–1 Thermal plumes and jets, and associated mixing and stratification phenomena in the SBWR.

3.2.1 Stratification and Mixing of the Suppression Pool

Possible stratification of the suppression pool is an important issue, since the temperature of the top layer of pool water determines the saturation pressure of the vapor in the gas space of the SC which, together with the partial pressure of the noncondensable gas, determines the containment pressure level.

The PCC vents inject noncondensable gases and steam into the SP at temperatures somewhat in excess of the SP water. Ideally, the steam condenses near the injection point. (Other possible situations, such as partial channeling of steam to the SP gas volume, are discussed in Section 3.5.2.) The SP may become stratified during the long term containment cooling phase, since the hot gases and the hot condensate will create plumes that will rise to the surface of the pool and spread horizontally.

3.2.1.1 Horizontal Spreading

The horizontal spreading of the hot plume on the pool surface takes place at a velocity having as order of magnitude the velocity of a gravity wave (e.g., Moody, 1990) given by

$$\sqrt{gH}$$

where H is the height of the "film" of hot water spreading on the colder pool surface. For a hot water layer of *only* 1 mm thickness, we obtain a horizontal spreading velocity of the order of 0.1 m/s. Thus, within a few tens of seconds at most, the hot water spreads on top of the pool up to the walls. This time is short compared to the time scale of containment response and *the horizontal spreading of the plume can be considered as being instantaneous*[b].

Consequently, at any instant, *the surface of the pool will have a temperature equal to the average plume temperature reaching the surface of the pool.* That temperature will depend on the dilution of the initial mass injected by the rate of entrainment of liquid into the plume from the colder pool (i.e., on plume behavior only).

3.2.1.2 Vertical Stratification

The layers of hot water spread on the surface of the pool will be displaced downwards by subsequent, hotter layers spreading on the surface (Smith et al.,

[b] This statement can be verified in the PANDA test facility where the hot plume rising from a vent in one of the SC vessels can spread towards the nearest vessel wall and also cross the large pipe connecting the two SC vessels and propagate in the second vessel, traversing a much larger distance, comparable to the circumferential distance between vents in the SBWR SC.

1992). This process will produce a degree of pool stratification, dependent, of course, on the amount of entrainment into the plume from the surrounding pool. With sufficiently large entrainment, the liquid reaching the surface of the pool will be only slightly above the pool average temperature, and the pool will be well mixed above the injection point.

If the entrainment into the plume is scaled properly (i.e., if the plume reaching the surface of the pool has the correct temperature history), it is evident that the correct scaling of the stratification (i.e., identity of the temperature gradients in a vertically 1:1 scaled facility or, alternatively, identical downward displacement velocity of the stratified fluid front) requires pool surface area to volumetric flow rate scaling:

$$(A_{LG})_R = \dot{J}_R = \dot{Q}_R = R$$

This condition already resulted from the top–down scaling considerations of Section 2. Thus, we will concentrate now on scaling of plume behavior.

3.2.2 Scaling of Plumes in Suppression Pool

Free plumes can be classified as laminar or turbulent. Geometrically, one distinguishes between axisymmetric round plumes and plane plumes. Thus, four different combinations exist (Gebhart et al., 1988). The scaling of plumes was recently discussed in relation to the SBWR by Peterson et al. (1993). Wall plumes (i.e., plumes rising around pipes or other vertical walls) provide lesser entrainment than free plumes (ibid) and should be avoided, if good mixing is desired[c]. Simple vertical pipe vents located near the vessel wall were, however, used in the GIRAFFE facility. Such vents will create wall plumes; this question is further discussed in Section 4.2.

The scaling of fully–developed plumes (i.e., plumes having self–similar radial distributions at various elevations), is relatively straightforward. The discussion of this section applies to such plumes. It is also assumed that the plumes do not interact with vessel walls and with neighboring plumes. This will be the case in sufficiently large–scale experiments.

In the following discussion, we consider first a **free, round, turbulent, buoyancy driven plume.** According to List (1982), at a given height z, the plume volume flow rate $\dot{J}(z)$ is given in this case by

[c] The PCC vents will be terminated by either horizontal quenchers distributing the gases essentially as a plane plume, or by a number of nozzles providing multiple free round plumes.

$$\dot{J} = k_{\mu} B^{\frac{1}{3}} z^{\frac{5}{3}} \tag{3.1}$$

where B is the specific buoyancy flux

$$B \equiv g \frac{\rho_a - \rho_o}{\rho_o} \dot{j}_o \tag{3.2}$$

k_{μ} a coefficient, and $\dot{J}_o$ the volumetric injection rate of mass at a density ρ_o, different from the ambient pool density ρ_a. In the case of steam condensing at the exit of the vent, $\dot{J}_o$ would be the resulting volumetric flow rate of condensate at temperature T_o injected into the pool at temperature T_a. The energy brought into the pool by the temperature increment $T_o - T_a$ will remain in the plume. The average temperature of the plume at an elevation z, T(z) can be obtained from an energy balance between the injection point and z:

$$\dot{j}_o(T_o - T_a) = \dot{J}(z)(T(z) - T_a) \tag{3.3}$$

Combining Equations 3.1 through 3.3, one obtains[d]

$$\frac{T(z) - T_a}{T_o - T_a} = \frac{\dot{j}_o}{\dot{J}(z)} = \frac{1}{k_{\mu}\left[g\frac{\rho_a - \rho_o}{\rho_o}\right]^{1/3}} \frac{\dot{j}_o^{2/3}}{z^{5/3}} \tag{3.4}$$

For prototypical fluids and identical temperatures between prototype and model, one concludes that

$$(T(z) - T_a)_R = \left(\frac{\dot{j}_o^{2/3}}{z^{5/3}}\right)_R \tag{3.5}$$

Thus, one finds out that when the vertical elevations are preserved,

$$(T(z) - T_a)_R = (\dot{j}_o)_R^{2/3} = R^{2/3} \tag{3.6}$$

and that, in general, the temperature of the plume reaching the surface of the pool will not scale properly, since $(T(z) - T_a)_R$ in the model will be smaller by a factor $R^{2/3}$ than in the prototype instead of being equal. Physically, this is mainly due to the fact that we are dealing with the behavior of a *point* source that is much weaker in the model. The buoyancy flux injected *at a point* fully determines plume

[d] The same dependence on $\dot{J}$ and z can be obtained following the scaling laws provided by Chen and Rodi (1980), Chapter 4.

behavior and cannot be scaled (at least when submergence is maintained): the lower buoyancy and entrainment provided by a weaker point source are only partially compensated by the corresponding reduction in the heat input.

However, it is most likely that the vent design of the prototype will spread the gases into the pool via a number of small vents or a quencher, producing essentially a **plane plume from a line source** by a linear arrangement of multiple nozzles. According to Equation 3.4, distribution of the gases in N nozzles, each having a volumetric flow rate $\dot{J}/N$, will reduce $T(z) - T_a$ by a factor $N^{2/3}$ and essentially promote mixing.

In this case, perfect scaling of stratification of the pool can be achieved by choosing

$$N_R = \dot{Q}_R = \dot{J}_R = R \tag{3.7}$$

In essence, this produces a scaled number of identical plumes in the prototype and the model.

In the case of a **linear quencher**, perfect scaling can be achieved by including in the model a scaled fraction of the total length of the quencher in the prototype. This produces in the model an identical segment of the prototype plume. In this case, the length of the quencher in the model should be scaled down by the system scale R.

If a design havin$_g$ **a few large vents** only is retained for the SBWR, there will be some unavoidable scaling distortion regarding pool stratification, according to Equation 3.4, unless one attempts to modify the plume height in order to have

$$(T(z) - T_a)_R = \left(\frac{\dot{j}_o^{2/3}}{z^{5/3}}\right)_R = 1 \tag{3.8}$$

or

$$(H_{sub})_R = (\dot{J})_R^{2/5} \tag{3.9}$$

It is unlikely, however, that good simulation will result since, for short plumes, the similarity conditions upon which the theories used above rely break down. The behavior of relatively short plumes is strongly affected by their initial developing region in a way which is difficult to analyze and scale. We have already seen in Section 2 that modifying the submergence depths distorts the thermodynamic behavior of the system. If the unlikely case that a few large vents are retained for the SBWR, this scaling difficulty could be resolved by conducting two series of

experiments covering submergence depths meeting *both* requirements. In one series of such experiments, the emphasis will be on pool stratification and in the second, on containment thermodynamics. Thus, a system code could be qualified regarding both aspects of the problem. This may not be required, however, if there is no significant stratification in the system due to efficient mixing by the vent plumes, as discussed below.

A variety of situations can be encountered, depending on the rate of injection of steam and noncondensables from the PCC vents. When the steam injection rates are high, one would expect stratification, in spite of better mixing of the pool by the higher entrainment rate, because of the larger source term, as shown by Equation 3.4. However, any amount of noncondensables present in the steam will strongly promote mixing by creating two–phase plumes. Two–phase bubbly plumes can be shown to be much more effective in mixing the pool than single–phase plumes (Coddington, 1993a). Information on entrainment in bubbly plumes is provided by several authors: Fannelop and Sjoen (1980) and Milgram (1983) also review previous work. Relevant information on the behavior of two–phase plumes related to aerosol pool scrubbing experiments was reported at a specialized meeting (Huebner, 1985). The directly related question of condensation of steam containing noncondensables injected from the PCCS vents is discussed in Section 3.5.2. In any case, the use of a scaled length of the prototype quencher in the test facility will lead to correct scaling of the mixing process.

3.2.3 Stratification and Mixing of Gases in the Drywell

A situation similar to the one presented in the previous section for plumes in the SP arises regarding hot or cold and/or steam or noncondensable–gas plumes in the DW. The geometry of the DW is relatively complex and the plumes can interact with structures, walls, etc. Releases from breaks in the primary system will create hot plumes or jets of steam; vacuum breaker openings will introduce plumes or jets of gases from the SC into the DW. Differences in the temperatures of vertical surfaces in the DW can produce rising hot and descending cold wall plumes; free plumes can be created by evaporation from the surface of pools of water. In relatively simple geometries, the correct scaling of such phenomena will be possible as long as the situation can be characterized by identical plumes or segments of linear plumes formed from nozzles or jets, both in the prototype and the models; this is the case of plumes created by a relatively large number of injection points or by linear sources.

For free round plumes, there is also the possibility of modifying the height of the fluid above the injection point and/or the volumetric flow rate per injection point to provide for correct scaling, according to Equation 3.5. The same dependence of

plume behavior on height and volumetric flow rate was obtained by Peterson et al. (1993), who also consider both buoyant jets and plumes, as well as the transition points between laminar and turbulent situations; consideration of the latter is also required for correct simulation of the plumes.

The elevations of the injection points could not be modified in the case of plumes in the SP considered in the previous section, since submergence of the vents had to be preserved. The absence of submergence preservation constraints in the DW opens the interesting possibility of modifying the elevation of the injection points in the models to better meet the scaling criteria using scaling criteria similar to the ones presented by Peterson et al. (1993); such scaling must be performed on a case–by–case basis.

The primary system **steam injection** situations that can be encountered in the DW of the SBWR are necessarily very diverse. The scaled experiments can also provide information about limiting envelope situations that can be used for code asessment.

The **vacuum breakers** can be visualized as horizontal disks, having a diameter of the order of 0.5 m, lifting under the pressure difference between the SC and the DW. Plumes from the vacuum breakers will likely inject gases at an angle close to the horizontal from the circular rim of these disks. Thus, to a good approximation, the jets/plumes from the vacuum breakers can be considered as linear sources having as length the perimeter of the vacuum breaker (Figure 3–1f). Correct scaling can be achieved by having in the models the scaled fraction of this perimeter.

3.3 Heat and Mass Transfers at Liquid–Gas Interfaces

Heat and mass transfers at liquid–gas interfaces (such as the surface of pools and of liquid films draining along the walls) depend on the interfacial surface area and on the variables driving the exchanges; namely, the state of the fluids at the interface and the hydrodynamic condition (i.e., the fluid velocities) near the interface.

The scaling of the **horizontal interfacial surface areas** was considered in Sections 2.2.2 and 2.4.3. The horizontal interfacial areas (e.g., pool surfaces) can be made to correctly scale with the system scale: $(A_{LG})_R = R$. The fluids used in the experiments and their thermodynamic states are prototypical. Thus, regarding mass transfers at horizontal interfacial areas, the only remaining scaling issue is the effect of the hydrodynamic conditions, i.e. essentially of the fluid velocities near the interfaces. This question is examined in Section 3.3.1 below.

The situation is different for **vertical interfacial areas** such as liquid films on the

walls. Phenomena taking place at vertical surface areas cannot be scaled accurately, since these areas cannot be scaled down exactly. More important, the heat transfers into the walls, which are often driving the interfacial mass transfers (e.g., condensation on liquid films along the walls), cannot be scaled either, due to the widely differing conduction heat transfer characteristics of the structures. However, they can be accurately estimated (see Section 3.4). Thus, we should only make sure that the vertical–interface phenomena taking place in the SBWR and its models are of similar orders of magnitude in relation to the heat and mass transfer phenomena which dominate *overall* system behavior. The data obtained from the scaled experiments can then be used to qualify the system code.

3.3.1 Interfacial Transfers at Horizontal Surfaces

The state of the fluids in the models being essentially prototypical, the temperature and concentration differences driving the interfacial exchanges should be very similar in the prototype and the models. The remaining question raised here is the effect of the flow conditions in the proximity of the interface on the heat and mass exchange *coefficients*.

The rates of condensation or evaporation on horizontal pool surfaces will be limited by diffusion of noncondensables or sensible heat transfer on the gas side and by heat transfer on the liquid side. No rapid circulation of either the water or the gases near the pool surface is expected (except in the presence of strong plumes reaching the surface, as discussed below). In most situations we may encounter rather stagnant flow conditions. If there is flow (on either side) parallel to the interface, the heat and mass exchange coefficients will depend on some fractional power of the Reynolds number (i.e., of the velocity of the fluids). It is not possible to make *general* scaling statements regarding such flows and their influence on the interfacial exchanges. No strong effects should be expected, however, unless some particularity of the design creates locally high velocities. Such questions should be examined case–by–case for all the facilities involved.

Strong single–phase or two–phase plumes reaching the surface of pools will spread horizontally and produce significant movement of the surface water. In this case the exchanges between the gas and the liquid spaces will be enhanced. Such phenomena will be properly scaled if the plumes themselves are scaled adequately (see Sections 3.2 and 3.5).

3.4 Heat Capacity of Containment Structures and Heat Losses

The walls and structures of the SBWR containment are complex composite structures with very large **heat capacity**. The massive reactor pressure vessel (RPV) is an additional source of stored heat. These cannot be easily simulated in scaled experimental facilities typically made of relatively thin–wall vessels, and no such attempt was made. One should remark, however, that the importance of both heat release from the RPV and of heat "soaking" into the containment structures decreases with time (as the structures come into temperature equilibrium with their surroundings and exchange less heat). Thus, for the long–term behavior of the experimental facilities considered here, heat exchanges with the RPV and the containment structures do not constitute the dominant heat sink.

More specifially, for the DW, in the long term, heat exchanges with structures are not important except to the extent that they may produce temperature gradients from one place to another, which may influence mixing. The amount of heat transferred to DW structures would be totally negligible compared to removal via the PCCS. In the SC, the situation is different; the outer containment wall can become a significant heat sink for energy that comes by heat conduction and bypass leakage from the DW.

Fitch (1993) used the TRACG Code to estimate the heat release from the SBWR RPV and its contents to both the primary coolant and to the air space in the DW. The calculations show that the heat release is essentially complete one hour after the beginning of depressurization. The overwhelming fraction of the heat (some 40 full–power seconds) is released to the primary coolant, while a small fraction (roughly 0.7 full–power seconds) goes directly from the RPV outer wall to the DW.

In the case of GIST, the water inventory in the RPV was increased to compensate for RPV metal heat release and arrive at an adequate simulation of level swell in the vessel (Billig, 1989). Heat release from RPV structures was not explicitly modeled in GIRAFFE. However, in view of the fact that the GIRAFFE tests are related to system behavior at least one hour after LOCA, this can be considered to be a minor effect. The same could be said for PANDA, but the decision was made to include it, since the necessary calculations are available and it is easy to accommodate the metal heat release through a small adjustment in the programming of the RPV electric heaters.

The **heat losses** from the systems considered are a directly related issue. Because of its much smaller volume–to–surface ratio and larger heat capacity, heat losses from the SBWR are relatively much smaller than from the experimental facilities. It is important to measure accurately the heat losses in the experimental facilities for application of the test data to computer code qualification.

Heat losses in GIST were not measured but, on the basis of engineering judgment, supported by computer calculations, are believed to be of second–order compared to the dominant energy transfers which govern the behavior of the facility. In the early GIRAFFE tests, heat losses were significant but were carefully measured and were compensated by an increase in the electric heater power. In the second series of GIRAFFE tests, efforts were made to minimize the heat losses by instaling guard heaters below the insulation on certain system components (Vierow, 1993). The heat losses during the PANDA experiments are expected to be relatively low and will be defined on the basis of extensive measurements. Additional discussion regarding the heat losses for the various experiments can be found in Section 4.

The concerns regarding any influence (on the overall behavior of the system) of heat storage and release from the RPV and containment structures and/or of heat losses from the experimental facilities are of significance only if such influences distort system behavior and lead to states of the system in the experiments which differ significantly from the expected behavior of the prototype.

It is important to note that the heat capacity of both the SBWR containment and of the corresponding parts of the experimental facilities, and the effects of transient heat conduction in the various structures and/or losses from the system, can be considered in computer calculations with a system code. Since conduction calculations are very well understood and can be performed with the necessary degree of spatial detail, and the thermal resistance is dominated by insulation with known properties, no significant uncertainty is expected in such calculations.

The conduction calculations need the fluid–to–wall heat transfer coefficient (h.t.c.) as input. The value of this h.t.c. is important and may be limiting the soaking rate during the initial period of transient heat transfer to wall and structures, during which the heat flux can be high. Afterwards, the heat flux into the walls and structures is usually limited by conduction, rather than convective heat transfer to the surface. Thus, although there may be some uncertainty regarding the condensation h.t.c. in the containment volumes, this uncertainty will not affect the calculated heat soaking rate.

In conclusion, the structure heat storage and heat loss issues for the experimental facilities *can be addressed adequately via data reduction and by the system codes* for both the SBWR and the experimental facilities.

3.5 Scaling of the Vents

The main (LOCA) vents will operate during the blowdown phase of the accidents considered; this phase is investigated in the GIST tests. The dynamics of **main vent clearing** is not an issue for GIST since vent flow is well established by the time the RPV pressure falls below the initial pressure of these tests. The main vents are not normally expected to open during the long–term containment cooling phase.

The PCCS vents will inject mixtures of steam and noncondensables into the SP starting with the blowdown phase and continuing thereafter.

The important phenomena that must be considered to understand the operation and consequently to properly scale the vents are:

(a) Flow regime and formation of bubbles at the vent.

(b) Creation of single– or two–phase plumes from the vents.

(c) Entrainment and mixing of fluid from the pool into the rising plume.

(d) Residence time of the two–phase plumes in the pool.

(e) Condensation rate of bubbles or jets containing noncondensables.

(f) Average temperature of the fluid in the plume as it reaches the surface of the pool.

Items c and f were already considered in Section 3.2. The remaining points related to the creation and behavior of two–phase plumes from vents are discussed in Section 3.5.2.

3.5.1 Number of Vents, Flow Area and Vent Hydraulic Diameter

The scaling of the number of vents and vent dimensions (up to the location of submergence in the SC pool) is covered by the general scaling criteria for the piping (Section 2.4.3). The geometrical configuration of the vents and their dimensions *at the submergence point* can clearly play an important role. Two limiting cases can be considered:

If the vent acts essentially like a point source of mass and energy in the pool, the analysis presented in Section 3.2.1 and in the following sections shows that it is practically not possible to design a scaled vent reproducing the behavior of the SBWR. On the contrary, if the actual vents are designed with multiple orifices or as "linear" sources of injected mass and heat, then their scaling is straigthforward: a fraction of the vent corresponding to the system scale R should be included in the experimental facilities (Section 3.5.2).

3.5.2 Condensation of Steam and Noncondensable Mixtures Injected from Vents into the Suppression Pool

The effects of vent design and scaling on pool stratification were discussed in Section 3.2.1. Moody (1986) provides information useful for the scaling of discharges from vents.

The start of GDCS injection essentially cuts off **main (LOCA) vent flow**. Regarding possible injection of steam and noncondensables from the main (LOCA) vents into the SP during the post–LOCA transient, submergence is the most important parameter and is conserved in all the tests.

Coddington (1993b) has reviewed the **PCCS venting phenomena**. This section summarizes the findings.

3.5.2.1 Creation of Bubbles at the Vents

The Laplace constant

$$\left(\frac{\sigma}{g(\rho_L - \rho_G)}\right)^{1/2}$$

determines the relative effects of buoyancy and surface tension σ in relation to bubble formation at an orifice. The experimental evidence (e.g. Wallis, 1969, pp. 244–247) shows that, for orifice diameters larger than the Laplace constant, the diameter of the orifice does not control the size of the bubbles produced. For saturated water at 0.2–0.5 MPa, the Laplace constant is of the order of 2.4 to 2.3 mm. In practice, vent orifice diameters are going to be larger than these values. For larger orifices[e], the bubble volume is given by

$$V_b = 1.138 \frac{j_G^{6/5}}{g^{3/5}}$$

where j_G is the volumetric flow rate of the gas through the orifice (Davidson and Harrison, 1963). The bubbles created at the orifice will likely be large enough to breakup into a swarm of smaller bubbles. Condensation of the steam should help break up the bubbles exiting from the orifices. Paul et al. (1985), in relation to pool scrubbing experiments, state that large bubbles will break up within 10 "globule"

[e] The diameter has to be smaller, however, than the minimum diameter for the so–called "total backflooding" or "weeping" regime (Bugg and Rowe, 1992). This limit is given by $D < j_G^{2/5}/(4g)^{1/5}$. When backflooding occurs, the bubbles are created *inside* the pipe. This limit will not be relevant when multiple–hole arrangements are used.

diameters to smaller bubbles with a log–normal distribution and a mean diameter of approximately) 5.8 mm. Coddington (1993b) estimates that the break up length can be of the order of magnitude of the SBWR PCCS vent submergence (nominally 0.75 m). The distribution of the bubbles created by breakup will depend on the Morton number of the fluid (e.g., Clift et al., 1978)

$$Mo \equiv \frac{\sigma^3 \rho_L}{g \mu_L^4}$$

where μ_L is the viscosity of the liquid. Clearly, for prototypical fluids, the Morton numbers, and consequently the bubble size distribution, will be preserved in the test facility.

3.5.2.2 Scaling of Two–Phase Plumes in the Pool

The residence time in the SP of bubbles created at the PCCS vents and containing a mixture of steam and noncondensables determines their degree of condensation. This residence time depends not only on the rise velocity of bubbles in stagnant liquid (of the order of 0.25 m/s for the bubble sizes — after breakup — considered here), but also on the influence of the void fraction in the two–phase plume and on the plume rise velocity, which, in turn depends on the rate of entrainment of liquid in the plume.

Preserving bubble size and plume characteristic dimensions (i.e., the plume source strength), as well as plume height, will also result in prototypical entrainment rates into the plumes; the plumes will be perfectly similar.

3.5.2.3 Condensation Rate of Bubbles or Jets Containing Noncondensables

Coddington (1993b) reviewed the literature on the condensation rate of steam bubbles containing noncondensables. He finds that the complete condensation time for pure–steam bubbles varies from 10 ms for small bubbles at high pool subcoolings up to 1 s for large bubbles in a low–subcooling pool. The addition of noncondensables increases the condensation time by up to a factor of 2. For small bubbles (2–mm diameter), the complete condensation time is much shorter than their residence time in the pool. For large bubbles, however (20 mm diameter), the bubble collapse time is comparable to its residence time. The residence time will, of course, be similar for essentially identical plumes.

3.5.2.4 Geometry of the Vents

We conclude that the behavior of the mixture of steam and noncondensables injected into the SP from the PCCS vents depends very much on the manner in which the total volumetric flow is distributed at the end of the vents. Within the range of volumetric flow rates of interest for the SBWR vents, the phenomena depend uniquely on the volumetric flow rate *per vent orifice*. In view of the dependence of individual bubble and two-phase plume behavior on bubble diameter, proper scaling of the vents is only possible when bubble dimensions are identical. Thus, it is possible to correctly scale the bubble generation and breakup phenomena at the vents, as well as the subsequent chain of phenomena, including condensation of the bubbles in the pool, *only when the vent orifice diameters are prototypical*. This is possible, for example, when a "linear" "line source" like vent arrangement is used. In this case, the plume in the model will simply be a segment of the plume in the prototype.

3.5.3 Vent Clearing, Chugging and Oscillations in the PCCS Vents

The dynamics of **main (LOCA) vent** clearing affect the peak containment pressure only during the early phases of blowdown. The main vents are not expected to open during the post-LOCA period, as already noted in Section 3.5. During the long-term decay heat removal period, any uncovery of the main vents will be driven by relatively *slow* increases in DW pressure and will be properly scaled by the correct submergence depths of the main vents.

The condensation of steam and noncondensable mixtures injected from the **PCCS vents** into the SP may lead to cyclic condensation phenomena. The scaling of vent geometry and dimensions and their effects on such phenomena were examined in Section 3.5.2. Proper scaling should be guaranteed if the vents in the experiments are a segment of the actual ("line source" vents) used in the SBWR.

A cyclic discharge of noncondensables from the PCCS vent was observed in GIRAFFE. Noncondensables apparently accumulate in the vent and the condenser tubes, the performance of the condenser degrades, the pressure rises and depresses the vent water level, the vent clears and discharges the noncondensables to the SP. The volume of the vent lines is likely to influence the period of this phenomenon (which is of the order of 100 s). Although the volume of the vent lines cannot be exactly scaled, as discussed in Sections 2.4.1 and 2.4.5, the scaling of the PANDA PCCS vent lines approaches the system scale (1:14 as compared to 1:25).

3.6 Heat and Mass Transfer in the ICS and PCCS Condensers

3.6.1 Condensation Inside the Tubes

The detailed database for low–pressure condensation heat transfer in the presence of noncondensables inside the PCC (or the IC) tubes is provided by the MIT and UCB single–tube data. These data were used to develop the condensation heat transfer model used in TRACG (Vierow and Schrock, 1991). The GIRAFFE, PANTHERS, and PANDA data provide mostly integral verification of the adequacy of this database. The GIRAFFE data were used to qualify the TRACG model (Andersen et al., 1993b). A limited number of local tube heat flux measurements are also foreseen for the PANTHERS tests.

Table 3–2 summarizes the ranges of the variables covered in the University tests and the corresponding expected ranges in the SBWR. It is evident that the single–tube data, obtained in tubes having prototypical dimensions, cover the range of interest.

Table 3–2

Parameter Range Comparison Between the Single–Tube Tests and the SBWR Conditions[e]

	SBWR	UCB–1[f]	UCB–2	UCB–3	MIT
Number of runs					
Pure steam		0	6	30	0
Steam/Air		30	30	50	52
Steam/Helium		0	18	20	22
Inlet pressure [psia]	40–70	4–65	13–44	16–75	16–70
Inlet temperature [°C]	120–150	72–146	95–134	95–150	100–140
Inlet steam flow rate [kg/hr]	6–40	6–25	16–73	30–60	10–33
Inlet air mass fraction	0–0.4	0–0.14	0–0.4	0–0.4	0.10–0.35
Tube dimensions					
Length [m]	1.8	2.1	2.44	2.44	2.54
Outside diameter [mm]	50.8	25.4	50.8	50.8	50.8
Tube thickness [mm]	1.65	1.70	0.71	0.71	2.40

[e] from Schrock (1992, 1993)
[f] basis for TRAC–G correlation

3.6.2 Heat Transfer on the Secondary Side

Heat transfer on the outside of the PCC (and IC) tubes (i.e., at the secondary side) is affected by the fluid and flow conditions in the pool. The single–tube UCB and MIT data were obtained with well–defined single–phase conditions on the secondary side.

In both the experimental facilities and the SBWR a (varying) number of tubes are used and the fluid and flow conditions in the IC pools need to be considered. In particular, the following should be considered:

- Effect of boiling on the secondary side.
- Effects of natural circulation in the pool.
- Effects of entrainment of fluid from the pool into the tube bundle.
- Flow patterns and void fraction distribution within the tube bundle.

Natural circulation within the IC pool is tested at full scale in the PANTHERS facility, which has a prototypical pool size. In the smaller–scale facilities (GIRAFFE and PANDA), natural circulation in the pool can only be approximated. Comparisons of single–tube (UCB and MIT), GIRAFFE, PANDA, and PANTHERS data will provide information regarding the importance of the natural circulation and bundle flow pattern effects.

Parametric calculations were also performed with a detailed analytical model of a condenser tube to clarify certain issues. This model treats a single tube as a counter–current flow heat exchanger with subcooled or boiling water flowing upwards on the outside and a mixture of steam and noncondensable gas flowing downwards inside (Meier, 1992, 1993). The model was used to assess the importance of the conditions on the secondary (pool) side on the overall heat transfer rate. The parametric studies (Meier, 1993) show that the overall performance of the condenser tube is not affected at all by the secondary–side mass flow rate (i.e., by natural circulation in the pool) when the pool water is saturated. This is the condition that will be encountered most during the tests. The secondary mass flow rate affects the overall heat transfer rate only as the subcooling in the pool (considered as the "inlet" temperature in the calculations) increases; the influence remains modest, as shown in Figure 3–2. Thus, no great influence of the effects of natural circulation in the pool is expected and scaling of this phenomenon is not a major issue for the test facilities.

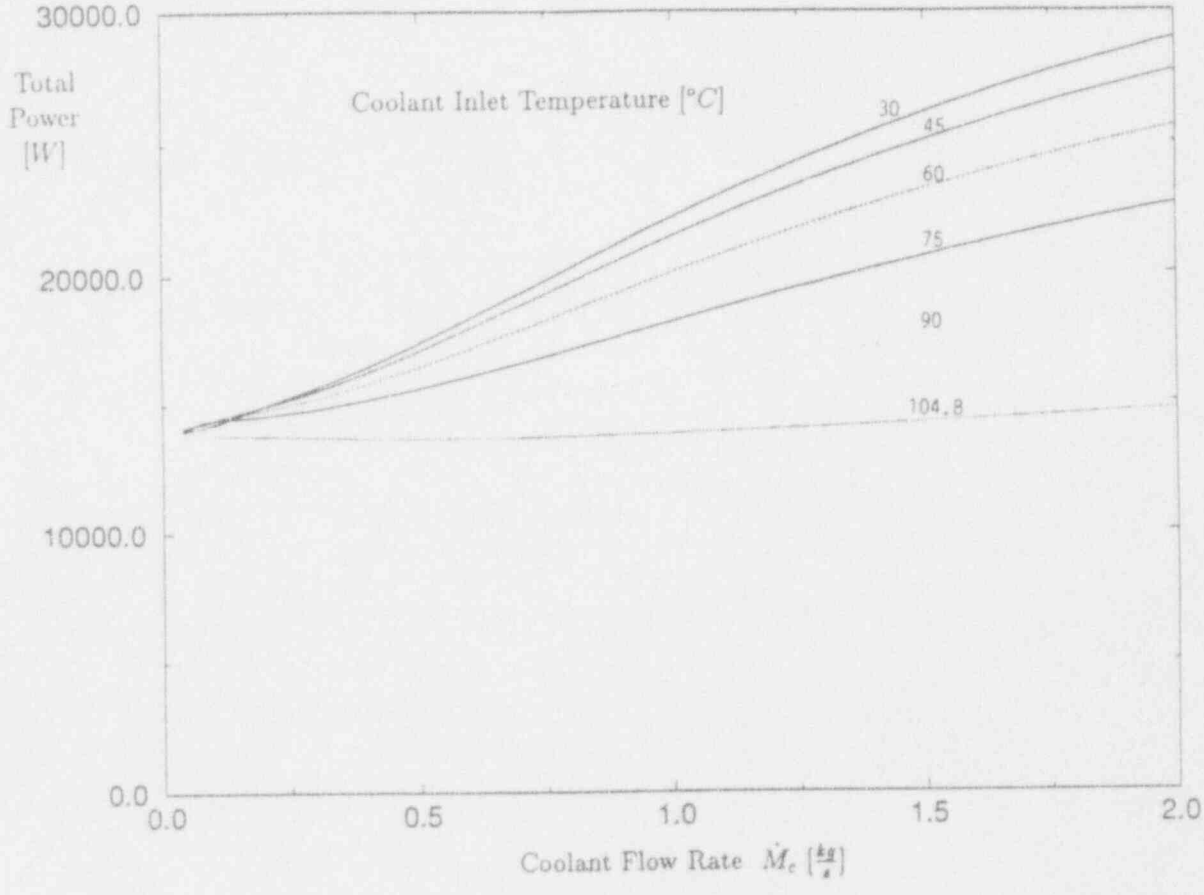

Figure 3-2 Effect of the Secondary Mass Flow Rate and Secondary Coolant "Inlet" Temperature on Condenser Tube Performance. [Calculations performed for the following typical conditions: pressure = 0.3 MPa; primary steam flow rate = 0.017 kg/s; nitrogen to steam ratio = 0.2; pool at 0.12 MPa.]

4. Scaling Approach for Specific Tests

The scaling approach followed in designing the various SBWR related facilities is briefly reviewed in this section, in relation to the main purpose of the tests. The use made of the data collected from these facilities to qualify the system code TRACG is discussed by Andersen et al. (1993a,b) and Kim et al. (1993).

4.1 GIST Tests

The purpose of the GDCS Integrated Systems Test (GIST) was to demonstrate the technical feasibility of the GDCS concept with scaled integral tests. The GDCS concept is based on the depressurization of the RPV to sufficiently low pressures to enable reflood of the core by gravity feed from an elevated pool. In particular, the tests were performed to show that the core remained covered under the most limiting design basis accident (DBA) conditions. The tests focused on system performance and on the coupled RPV–containment response for the low pressure (below 0.79 MPa) range of the LOCA blowdown phase.

More specifically, the GIST test objectives were to:

(1) Show the technical feasibility of the GDCS concept by performing a section–scaled integrated systems test of the SBWR design.

(2) Provide an additional database to qualify the TRACG code[a] for use in SBWR accident analyses.

(3) Provide data for refinement of the models available in the computer code TRACG to realistically predict the SBWR response to postulated LOCAs using GDCS injection for reactor makeup water.

When the GDCS operates, the gravity drain flow rate to the RPV depends on the piping geometry, the state of the fluid, and the pressure conditions in both the GDCS pool and the RPV. Flow entering the vessel during the later stages of blowdown during a postulated LOCA must be sufficient to keep the core flooded. The GDCS flow and core flooding phenomena *could* be studied in separate–effects tests if they were relatively decoupled. However, the degree of coupling could be better quantified with an integral test which included both flow from the GDCS pool

[a] The TRACG models that are relevant to GIST had already been qualified by other tests such as TLTA, FIST, etc (Andersen 1993a,b).

and flooding of a modeled vessel with a representative decay heat rate. Therefore, the GIST tests were designed to test the technical feasibility of the gravity drain process during and after system blowdown.

The GIST facility was built at the GE Nuclear Energy site in San Jose, California. All significant plant features which could affect the performance of the GDCS were included (Billig, 1989; Mross, 1989). Since the containment pressure and the GDCS pool water level determine GDCS activation, the containment (both upper and lower DW and SC volumes) was modeled. The facility is schematically shown in Figure 4–1. It is a 1:508 volumetric–scale, section model of the March 1987 SBWR conceptual design. Vertical elevations are scaled 1:1. Subsystem horizontal areas are also scaled according to the system scale of 1:508, except for the drain flow lines, as discussed in Section 4.1.2.1 below. Decay heat was modeled in proportion to the 1:508 system scale to provide the correct depletion of liquid water from the RPV by boiling (Billig, 1989).

The scaling of the tests produced data at real time and at prototypical pressures and temperatures. Detailed descriptions of the design and operation of GIST can be found in Mross (1989).

GIST has cylindrical vessels interconnected by piping simulating the various volumes of the SBWR, i.e. the RPV, upper DW, lower DW, and elevated SC (filling also the role of GDCS pool). The piping includes simulation of the Automatic Depressurization System (ADS), the GDCS lines, and the conditions at the break location for all break types considered (Billig, 1989).

The range of 24 tests conducted included Main Steam Line Break (MSLB), GDCS Line Break (GDLB), Vessel Bottom Drain Line Break (BDLB) and no–break (NB) transient tests.

During the GIST tests, the system was first depressurized to the atmosphere from its initial pressure of 1.07 MPa to 0.79 MPa. This period of the tests was thus used to create representative initial conditions in the RPV, as it entered the later stages of the depressurization transient (Figure 4–2). The initial conditions of importance are the decay heat generation rate, and representative water levels and void fraction distributions in the RPV. When the RPV reached the pressure level of 0.79 MPa, the blowdown flow rate was switched from the atmosphere to the DW for the break flow line, and to the SC for the ADS lines. Care was provided to obtain a smooth transition by not introducing changes in the blowdown flow areas.

With further depressurization of the RPV, the low pressure DPVs open. Eventually, the head of water in the SP becomes sufficient to overcome the RPV pressure and open the GDCS check valves allowing GDCS flow to enter and reflood the vessel.

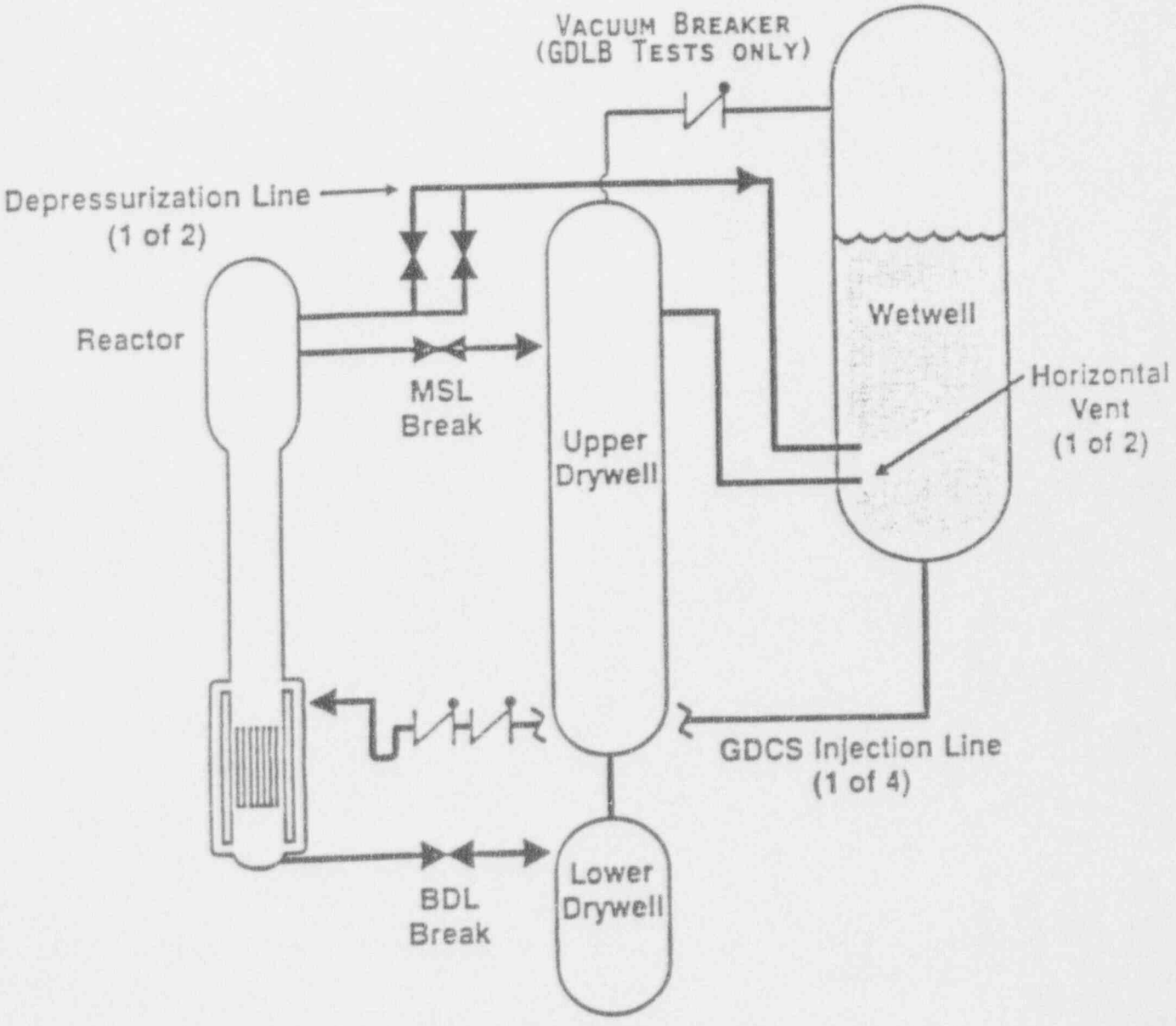

Figure 4–1 Main Components of the GIST Facility

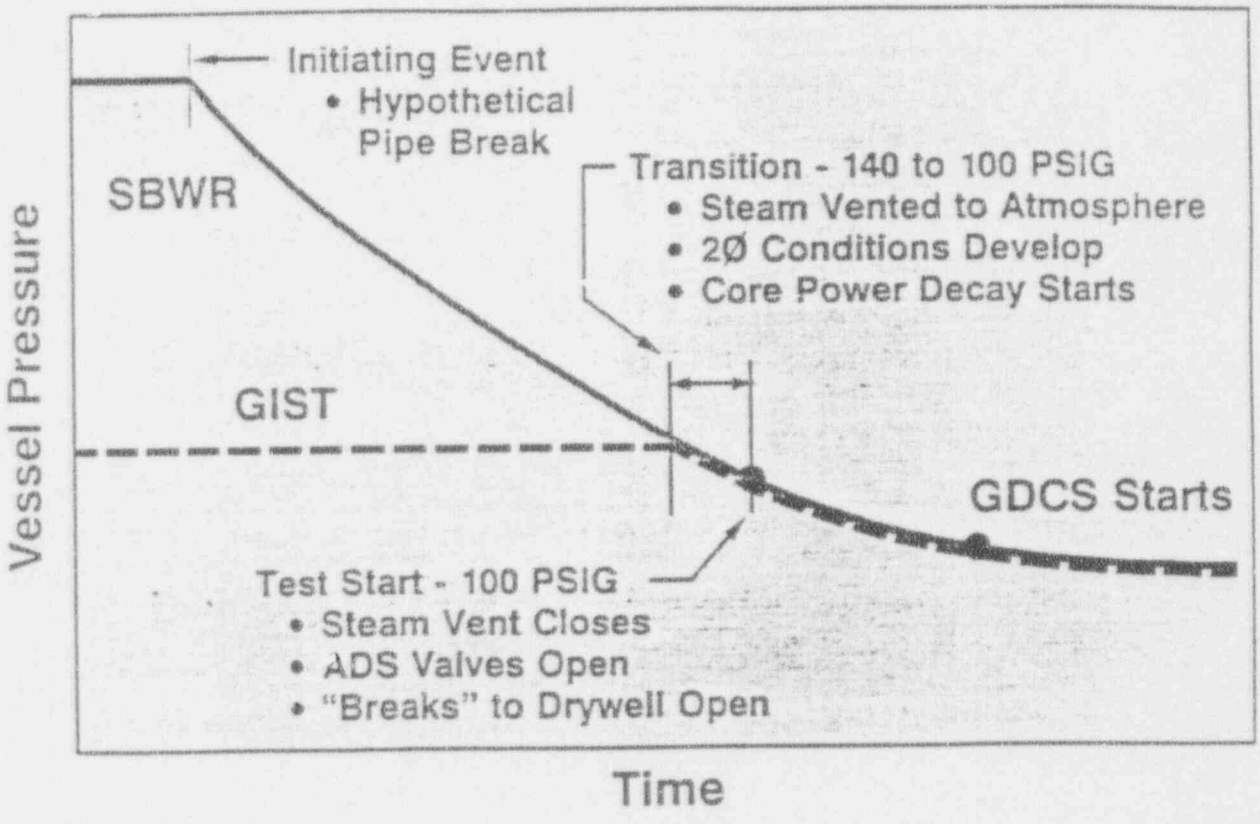

Figure 4–2 Vessel Pressure Coastdown During the SBWR and the GIST Depressurization Transients

4.1.1 General Scaling Approach

The design of the experimental facility is in agreement with the general top–down scaling criteria derived in Section 2. The bottom–up scaling of certain phenomena identified by the SBWR PIRT (Table 3.1) is discussed in Section 4.1.2 below.

The feasibility of the GDCS system would be demonstrated if it delivered sufficient core flooding flow during various LOCAs. The overall "global" system effects of pressure and RPV water inventory history during the LOCA had clearly to be

modeled in a top-down fashion to include representative coupling effects of the GDCS flow with the RPV inventory. The GIST tests provided representative data that were used to qualify the TRACG code (Andersen et al., 1993). The particular phenomena not scaled in detail are not expected to produce bifurcations in system behavior invalidating the representativeness of the tests, or bringing the experimental apparatus outside the range of conditions expected in the SBWR; the differences are, furthermore, captured adequately in code calculations (Billig, 1989).

Billig (1989) discusses the limitations and scaling of the GIST tests; the Appendix of the report describes all the differences between the design tested and the final SBWR design, their impact on system performance, and justifies the validity of the GIST tests for SBWR applications.

As noted earlier, LOCA blowdown pressure history was simulated from a RPV pressure of 0.79 MPa, since the GDCS begins to function at lower pressure. The pressure-time characteristics were controlled by adjusting the flow area in the blowdown pipe for the various accident scenarios simulated.

4.1.2 Particular Scaling Issues for the GIST Tests

4.1.2.1 Exact Scaling of the SBWR Geometry

There are a number of geometrical distortions in the GIST facility. These are due to the fact that the SBWR simulated design was not the final one; to the one-dimensional character of the facility and the relatively small horizontal-area scale of the system; and to the particular design choices of certain facility components. The experimental GIST results were used to qualify TRACG for SBWR analysis (Alamgir et al. 1990; Andersen et al., 1993b). Given the approach and limitations mentioned above, the GIST results should be viewed as having provided, in addition to a demonstration of the GDCS concept, additional data for code qualification. Most of the test limitations and particularities, as well as the code qualification work, were discussed already in detail by Billig (1989); this discussion is not repeated here. Only certain issues, such as the determination of the initial test conditions, are discussed below. Certain geometrical differences between the GIST facility and the final SBWR design are also discussed. Their impact was addressed by Billig (1989).

The major difference between the 1987 and final SBWR designs is that, in the earlier version, a single pool was used to provide both containment pressure suppression and the source of the GDCS water, Fig. 4-3. In the final SBWR design, the water inventories for GDCS and pressure suppression are separated. The suppression pool is in the SC and the GDCS inventory is equally divided among

three pools located on the diaphragm floor within the DW. A second difference is the addition of six DPVs discharging directly to the DW, to supplement the ADS function performed by the SRVs discharging to the SP.

An important parameter determining reflooding of the vessel is the upward force acting on the gravity head of the coolant in the downcomer. This depends on the pressures in the RPV steam dome and at the GDCS flow injection point. The differences in the older design tend to *inhibit* GDCS injection in GIST, relative to what would be expected in the present SBWR. This can be understood by recognizing that the DW and SC pressures in the SBWR are *not* independent variables, Fig. 4–3. During the entire blowdown, the DW pressure exceeds the SC pressure by, at least, the hydrostatic head required to open the top LOCA vent (about 15 kPa). This means that the GDCS pool overpressure in GIST was actually lower, relative to the RPV pressure, than it would be in the plant. (Alternatively speaking, the pressure in the RPV steam dome was higher). Blowdown through the DPVs in the SBWR tends to sustain LOCA vent flow and ensures that DW pressure remains above SC pressure up to the time GDCS flow initiates. The top of the GDCS pool, which is directly connected to the DW will, therefore, be at a relatively higher pressure in the current SBWR.

The presence of the PCCS condensers in the SBWR will have a small effect on the *absolute* pressure in the DW, but will not change much the pressure *difference* acting to reflood the vessel. Similarly, the ICS condenser loop, absorbing some steam from the RPV dome, will tend to reduce the absolute pressure in the RPV but not the pressure difference causing reflood.

In summary, the combined effects of PCCS and ICS operation and of having separate GDCS pools in the SBWR DW may alter the absolute pressure in the RPV, but are expected to have minimal influence on the pressure difference driving the flow reflooding the vessel. The absolute pressure changes are small and are not expected to create atypical thermodynamic conditions. Finally, in judging the effect of differences between GIST and the final SBWR design, it is important to note that the key GIST parameters (i.e., RPV and GDCS water levels and containment pressure) were either representative or conservative relative to the final SBWR design. The key parameters were also varied over a sufficiently broad range to allow detailed qualification of the TRACG code.

The **GDCS drain line flow area** modeling was conducted according to the general top–down criteria of Section 2.4.5. The SBWR drain line flow areas were increased after the GIST facility was built. Since the drain flow rate depends on both the line area and flow resistance, it was possible to employ the original model pipes with orificing loss coefficients reduced (orifices removed). This resulted in a representative drain flow into the RPV, in line with the scaling described in Section 2.4.5: the

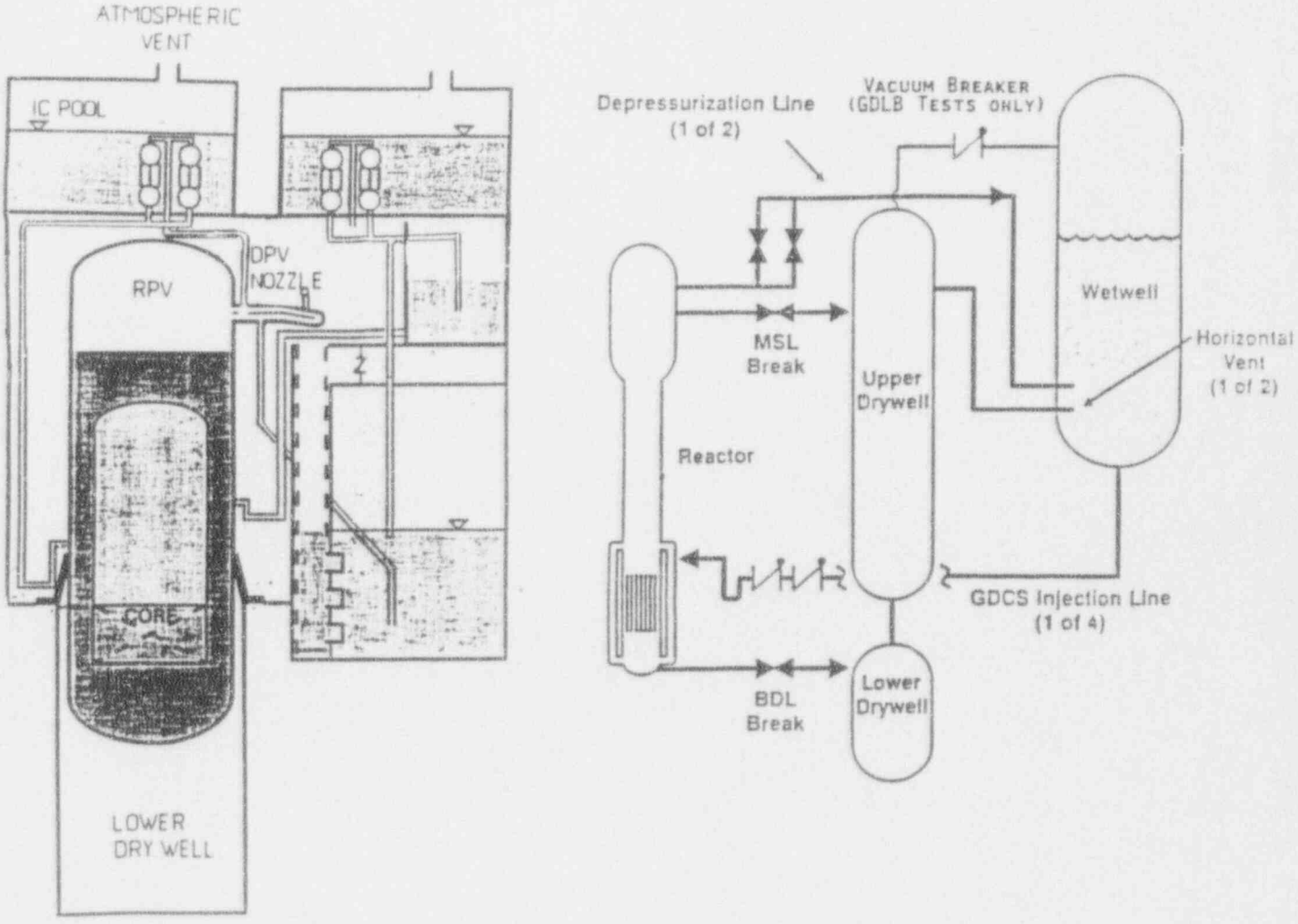

Figure 4–3 Flow Paths During the Late Blowdown Period in the SBWR and in the GIST Facility During a MSL Break

transit time of the fluid in the GDCS lines is short compared to the RPV filling time; as long as the flow rate remains representative, flow line modeling distortions related to transit time are acceptable.

Heat losses from the GIST facility were controlled by surface insulation. The losses were not measured, but, with the insulation used in the facility, they are estimated to be of secondary importance in relation to the major top–down–scaled energy transfers in GIST. For well insulated vessels, the estimation of the heat losses is relatively insensitive to uncertainties in the ambient convection heat transfer coefficient. The uncertainty in the heat loss estimation must be considered in code simulations of these tests.

4.1.2.2 Establishment of Representative Initial Conditions

The initial test conditions for the GIST tests were determined from TRACG simulations of the early blowdown behavior of the SBWR from 7 MPa to 1.07 MPa. For the tests, the system was first depressurized to the atmosphere from this initial pressure of 1.07 MPa to 0.79 MPa. Thus, this period of the tests was used to create the representative initial conditions in the RPV as it entered the later stages of the depressurization transient, as shown in Figure 4–2. The pressure dropped from 1.07 to 0.79 MPa in 30 to 50 seconds (Billig, 1989); this provided sufficient time for representative conditions in the RPV to develop.

The vessels representing the containment were pressurized and preheated to the TRACG calculated pressures and temperatures. The DW was purged of air with steam to simulate the effect of air carryover into the SC.

Initial pool water temperatures in the GIST tests were controlled by heating prior to system blowdown. The initial temperatures ranged from 42 to 69 C, which embraces possible initial conditions in the SBWR.

The GDCS check valves, which open only when RPV pressure reaches a predetermined level, were not required to provide exact opening time characteristics, because the actual opening time is rapid relative to the vessel filling time.

The heat release from the RPV metal could not be simulated in the GIST tests; the heat stored initially in the RPV wall and its rate of release could not be scaled properly. Thus voids could not be maintained in the lower plenum and the water level in the core dropped; this was compensated by increasing the initial RPV water level in the tests. This distortion can be considered in TRACG calculations which can simulate the situation in the tests and in the SBWR.

4.2 GIRAFFE Tests

The GIRAFFE test facility (JAPC et al., 1990; Nagasaka et al., 1991; Yokobori et al., 1991; Vierow, 1993) is a full-height, reduced volume, integral system test facility, built by Toshiba at its Kawasaki City, Japan site, to investigate various thermal-hydraulic aspects of the SBWR passive heat removal systems, to demonstrate that the PCCS satisfies its design criteria in support of design certification, and to provide data for TRACG code qualification.

The facility consists of five major components representing the SBWR primary containment and IC pools, the PCCS condenser, and the connecting piping. Separate vessels represent the RPV, the DW, SC, GDCS pools, and ICS pools, which house the PCCS condensers. A schematic of the facility is shown in Figure 4-4 and details of its isolation condenser are shown in Figure 4-5. The facility scales the SBWR at a volumetric scale of 1:400. The heights and vent submergences are scaled 1:1. Pressure and temperature levels and pressure drops are preserved.

The objective of the GIRAFFE test program was to provide separate effects and integral data for qualification of TRACG. The **separate effects tests** address the issues of steam condensation heat transfer rates from a steam-nitrogen mixture under steady-state conditions, and of venting of noncondensable gases via the passive containment heat exchangers (PCCS system) to the SP. The **integral tests** demonstrate the concept of the PCCS for decay heat removal and provide data for a variety of LOCA simulations, against which computer codes for post-LOCA containment analysis may be qualified. Details of the scaling of the GIRAFFE facility and of the instrumentation are provided in the references cited above.

Data from separate effects condensation tests were obtained at a pressure of 0.3 MPa, for steam flow rates of 0.01 to 0.04 kg/s and nitrogen partial pressures of 0.0 to 0.03 MPa. The initial conditions for the noncondensable venting and long-term integral tests corresponded to those at one hour from the initiation of a LOCA. For the venting study, the nitrogen vent line of the PCC unit was submerged at depths of 0.4, 0.65, and 0.90 m, thus covering the range of interest for the SBWR.

The main steam line break, GDCS line break, and bottom drain line break LOCAs were simulated during the long-term system response tests.

4.2.1 Scaling of the GIRAFFE Facility

The detailed description of the facility can be found in the report by Vierow (1993), which is the basis for the following discussion. To comply with top-down scaling criteria, the GIRAFFE facility has been constructed on a 1:1 height scale to the

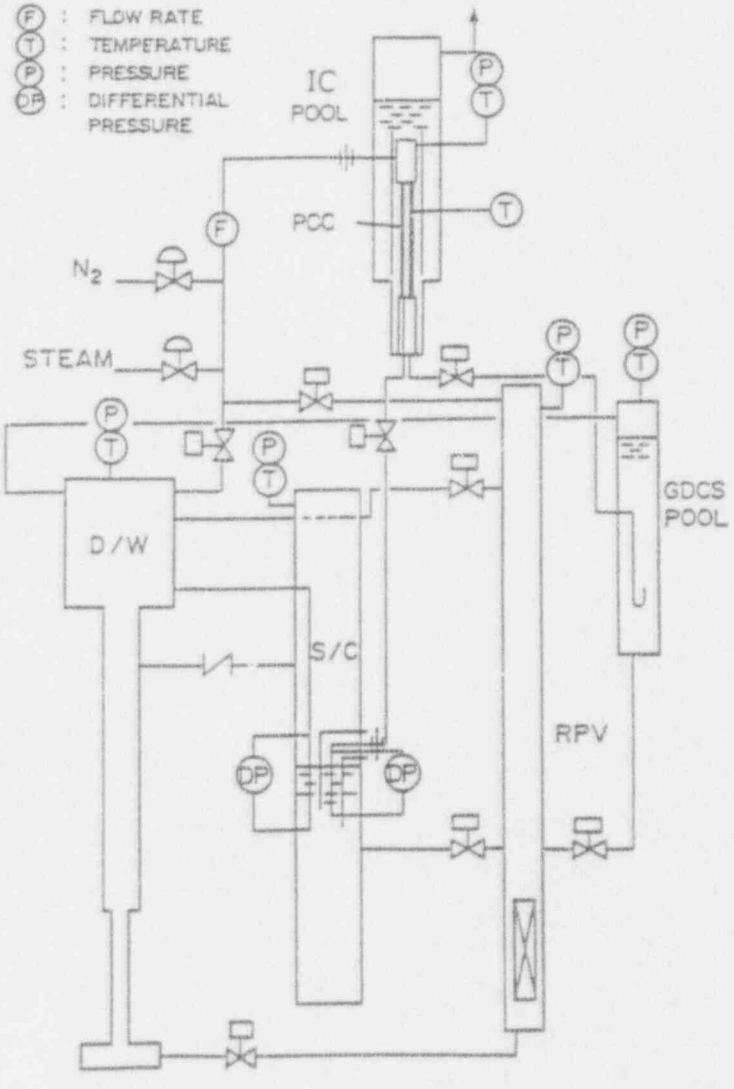

Figure 4–4 Schematic of the GIRAFFE Test Facility (Phase–2 Configuration)

SBWR design, and all essential elevation differences between the various vessels and between corresponding SBWR components have been preserved (Yokobori et al., 1991). The system scale for volumes, power, horizontal areas, and mass flow rates is 1:400. The RPV heater produced power according to a decay heat curve plus a constant amount, added to compensate the heat losses from the system (Vierow, 1993).

The RPV is simulated in full height from the bottom of the core up to the MSL exit, with the RPV–to–PCC and RPV–to–GDCS pool elevation differences conserved. The volumes above this full–height–simulation region have been shortened, but their volumes have been included in the volume of the RPV, which is scaled according to

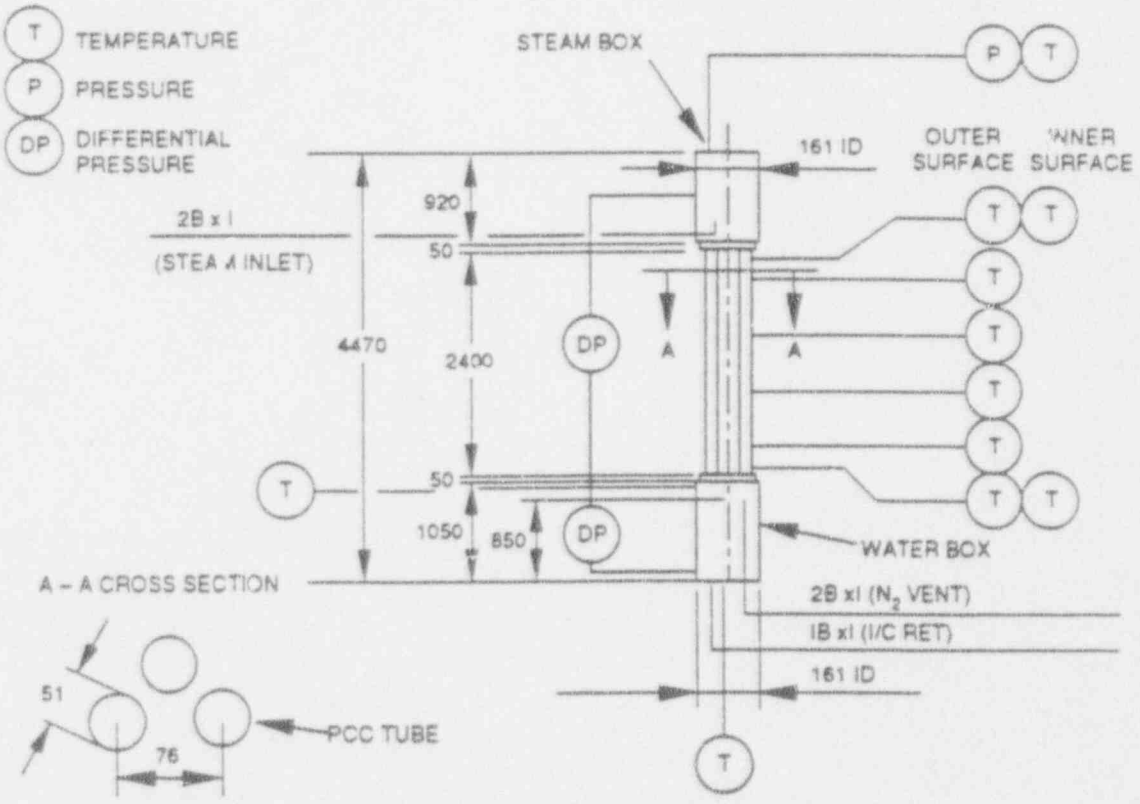

Figure 4–5 Details of GIRAFFE Isolation Condenser

the system scale of 1:400. The electrical heat input to the simulated core is also scaled 1:400.

The DW is also nearly full-height, with only the upper- and lower-most regions shortened. The volumes and areas are scaled down 1:400, and the cross-sectional area variation with height is preserved, so that the DW water level transient is similar to that expected in the SBWR under LOCA conditions. Although the annular shape of the SBWR DW could not be accommodated in GIRAFFE, the facility includes compartments that can be associated with the various regions of the SBWR drywell (Figure 4–4). The lower larger drywell volume, which represents on a 1:400 system scale the corresponding SBWR volume, can retain noncondensable gases and/or water. There is also a connection to a steam injection line, which is used to

simulate evaporation from accumulated water. The narrowest region, representing the annular DW space around the RPV in the SBWR, has a correctly-scaled cross-sectional area; thus, water level changes in the DW occur at prototypical rates. A vacuum breaker line connects the annular DW to the SC gas space. Connections to the main steam line, the main LOCA vent line, the GDCS air space, the DPV line, and PCC steam supply line correspond to those in the prototype SBWR.

The full height of the SC has been preserved, while the gas and water volumes have been again scaled down 1:400. The LOCA vent line is at its actual SBWR elevation. The vertical section of the main LOCA vent is a close-ended pipe extending from the upper DW almost to the SC floor; each of the three holes in the pipe wall representing the main vents has the proper size and elevation. Three alternative PCC vents, each with a different submergence depth, were installed in the SP to allow the study of submergence effects. These vents are vertical pipes with open ends, installed near the vessel wall.

The GIRAFFE vacuum breaker connects the annular region of the DW to the gas space of the SC, as shown in Figure 4-4. This particular connection must be considered in code simulations of the system.

The GDCS pool has exactly scaled height and volume.

The GIRAFFE isolation condenser is a scaled representation of the three SBWR PCCS condensers; the GIRAFFE condenser has three tubes (Figure 4-5). This unit is somewhat different from the most recent PCCS condenser design, with a longer condenser tube length (2.4 vs 1.8 m) and vertical, cylinder-shaped inlet steam and condensate collector boxes. The tube wall thickness is 2.5 mm, compared to the 1.65 mm wall thickness of the SBWR PCC units. The total surface area of the condenser tubes in GIRAFFE is scaled by 1:372 or 1:386, based on the outside or inside tube diameters, respectively. This is sufficiently close to the system scale of 1:400, considering the fact that 1.8 m is the minimum length of the SBWR PCCS tubes. The three GIRAFFE condenser tubes are spaced as to maintain correct secondary-side cross-sectional flow area.

Matching the condenser tube surface area with tubes of different length does not provide *a priori* proper scaling. For moderate differences in length, however, the shorter length is compensated by the redistribution of the total available flow to the tube array. This was confirmed by calculations with the detailed analytical model (Meier, 1992, 1993) of a condenser tube mentioned in Section 3.6.2. The calculations showed that three 2.4 m tubes perform in a practically identical fashion as four 1.8 m tubes having the same total heat transfer area; deviations in the total heat transfer rate remained within 2 % over a wide range of operating conditions.

The IC pools house the PCC unit, which is placed within a chimney separating the region where the water is in contact with the PCC tubes from the outer pool region; this provides for simulation of the circulation in the IC pool. As stated in Section 3.6.2, the total heat transfer rate from the condenser tubes is relatively insensitive to the circulation pattern on the secondary side. There is enough water in the IC pool for three days of decay heat removal.

The initial test series in GIRAFFE were run with the PCC draining liquid directly to the RPV, while in the later series the present SBWR configuration (draining via the GDCS pool) was implemented. Such differences have a minimal effect on GIRAFFE's ability to study the PCCS phenomena and, furthermore, the differences can be easily accounted for in code calculations.

All lines are sized and orificed as to allow for prototypical pressure drops at scaled mass flow rates; the pipes are somewhat oversized with respect to the system scale. This reduces the frictional pressure drops, and the total resistance of each line is adjusted by inserting an orifice plate representing the appropriate loss coefficient. The adequacy of this scaling was discussed in Section 2.4.5.

4.2.2 Particular Phenomena of Relevance to the GIRAFFE Tests

4.2.2.1 Heat Losses from the Experiment

The GIRAFFE vessels, piping and flanges were insulated. The heat losses were measured under a variety of ambient conditions and are known to within a few percent. The heat losses from the RPV and connecting lines were compensated by increasing the power to the RPV heating element (Vierow, 1993).

In later tests, microheaters were installed on the GDCS, DW and SC vertical walls and on the SC roof beneath the insulation. The power to these heaters was regulated by a microprocessor, so as to maintain thermocouple pairs on the inside and outside of vessel walls at the same temperature and stop the heat loss.

4.2.2.2 Storage of Noncondensable Gas in the Lower DW

Relatively colder nitrogen may "fall" and possibly accumulate in the lower DW during certain phases of the simulated transients. This nitrogen may be subsequently convected upward, to alter the composition of the mixture entering the PCCS condenser, and consequently its performance. Nitrogen returned from the SC to the DW by opening of the vacuum breakers may also sink to the lower DW. The distribution of the noncondensables in the various DW regions is also affected, however, by any heat released from the RPV in the annular space surrounding it

and by heat transfer to the colder vent wall; these details were not simulated in GIRAFFE. Water spilling from the DPVs tends to mix the DW gases and creates a saturated pool, which promotes upwards motion of the nitrogen. This effect was observed in GIRAFFE testing (Vierow, 1993).

A number of tests were run at the GIRAFFE facility to investigate the distribution and mixing of nitrogen in the DW and collect data for qualifying the TRACG Code (Vierow, 1993). These tests include a case with steam supply to the lower DW simulating the evaporation of water accumulated there. Special procedures were followed to charge the DW with various spatial distributions of noncondensable gas. Some DW mixing occurred prior to the start of the tests; to capture such pre-test mixing, the injection process must also be modeled in the computer simulations (Vierow, 1993).

4.2.2.3 Scaling of the PCCS vents

As noted earlier, the GIRAFFE PCCS vents are round open pipes located near the vessel wall. They are likely to create wall plumes. As discussed in Section 3.5, this does not provide accurate scaling (in relation to a straight-pipe prototypical full-scale vent) for the single- or two-phase plumes emerging from the vents and for mixing in the pool. The comparison should be made with the final design of the SBWR vents.

4.3 PANDA Tests

The PANDA test facility, which is nearing completion, will be used to conduct integral system tests, as part of the ALPHA program at the Paul Scherrer Institute (PSI) in Switzerland (Coddington et al., 1992). It will demonstrate PCCS performance on a larger scale than GIRAFFE. The facility has a full 1:1 vertical scale, and 1:25 "system" scale (volume, power, etc). It is primarily intended to examine system response during the long-term containment cooling period. The overall objectives of the PANDA tests are to demonstrate that:

(1) the containment long term cooling performance is similar in a larger scale system to that previously demonstrated with the GIRAFFE tests,

(2) any non-uniform spatial distributions in the DW or SC do not create significant adverse effects on the performance of the PCCS, and

(3) there are no adverse effects associated with multi-unit PCCS and ICS operation.

The tests will also extend the database available for computer code qualification.

The initial test series at PANDA will consist of two main steam line break (MSLB) tests. The first will be similar to the GIRAFFE MSL break with uniform DW conditions, while the second is planned in a manner maximizing the influence of DW asymmetries on the operation of the PCCS condensers.

Uniform and asymmetric DW conditions can be created in PANDA through the capability to vary the fraction of break/DPV flow which is injected into each of the interconnected DW vessels. The steam condensing capacity directly connected to each vessel (i.e., the number of condenser units) can also be varied. Finally, steam and/or noncondensables can be injected at various locations in the DW vessels to study mixing phenomena and to provide envelope information for the corresponding SBWR conditions.

4.3.1 Conceptual Design

Early during the conceptual design phase of the facility, it was recognized that it is neither possible nor desirable to preserve exact geometrical similarity between the SBWR containment volumes and the experimental facility (Coddington et al., 1992). On the other hand, multidimensional containment phenomena such as mixing of gases and natural circulation between compartments may depend on the particular geometry of the containment building. The general philosophy followed in designing the experimental facility was to allow such multidimensional effects to take place by dividing the main containment compartments in two and by providing a variety of well–controlled boundary conditions (e.g., inbalances) during the experiments, so that the various phenomena could be studied under well–established conditions, and a behavior envelope of the system established. Carefully conducted parametric experiments will also provide more valuable data for code qualification, rather than attempts to simulate geometrically, but to a necessarily limited degree, the rather complex reactor system. Boundary conditions and the behavior of the interconnections between containment volumes can be controlled to study various system scenarios and alternative accident paths.

Thus the RPV and the GDCS pools are represented each by a vessel. The DW and SC are represented both by two separate, interconnected vessels, (Figure 4–6). The RPV contains a 1.5 MW electrical heat source. There is a total of three PCCS condensers representing the corresponding three units in the SBWR and a single ICS condenser representing two of the three SBWR units. (The two ICS condenser units correspond to the 2 x 50 % design value of the cooling capacity; the third ICS condenser is an extra 50 % redundant unit). The condensers are connected to the two DW vessels, as shown in Figure 4–7. The fact that there are three PCC units and

only two DW volumes will allow some degree of asymmetric behavior or create flows between the two DWs, even with equal flow areas from the RPV to the two DW volumes.

The details of the system and its scaling rationale are described by Huggenberger (1991a, 1991b, 1992, 1993a, 1993b), Coddington (1992), and Coddington et al. (1992). Figure 4–7 shows details of the piping interconnecting the various volumes. The facility is heavily instrumented with some 560 sensors for temperature, pressure, pressure difference, level or void fraction, mass flow rate, gas concentration (humidity or air content), electrical power, and conductivity (presence of phase) measurements (Dreier, 1992).

4.3.2 Scaling of the PANDA Facility

The scaling of the facility conforms to the top–down and bottom–up criteria developed in Sections 2 and 3 of this report. Full vertical heights and submergences are preserved to correctly represent the various gravity heads; volumes are represented at the system scale. The exceptions to these are noted below (Huggenberger, 1991a, 1993a). The experiments will be conducted under reactor pressure and temperature conditions which are prototypical for the phase of the accident under consideration.

4.3.2.1 Volumes

Figure 4–8 shows the geometrical arrangement of PANDA in comparison to the SBWR and the relative elevations of the two systems. All the SBWR heights are represented except those below the Top of Active Fuel (TAF) in the core. The top of the PANDA RPV electric heaters is placed at the TAF location; the heaters are, however, shorter.

In the RPV, the liquid inventory above the Bottom of Active Fuel (BAF) is scaled according to the system scale of 1:25. The *liquid inventory below BAF in the RPV* was eliminated (Figure 4–8), since it remains saturated and essentially inactive during the post–LOCA phase of the accidents considered, and is not required for the correct simulation of gravity heads. The *liquid volume between mid–core and BAF* is included, however, in the scaled PANDA RPV volume by a small adjustment of the vessel diameter (Huggenberger, 1993a). The lowest SBWR line simulated in PANDA is the equalization line which enters the RPV at one meter above TAF. Thus eliminating and redistributing the water volume below mid–core and modifying the length of the heater elements will not influence significantly any natural circulation paths.

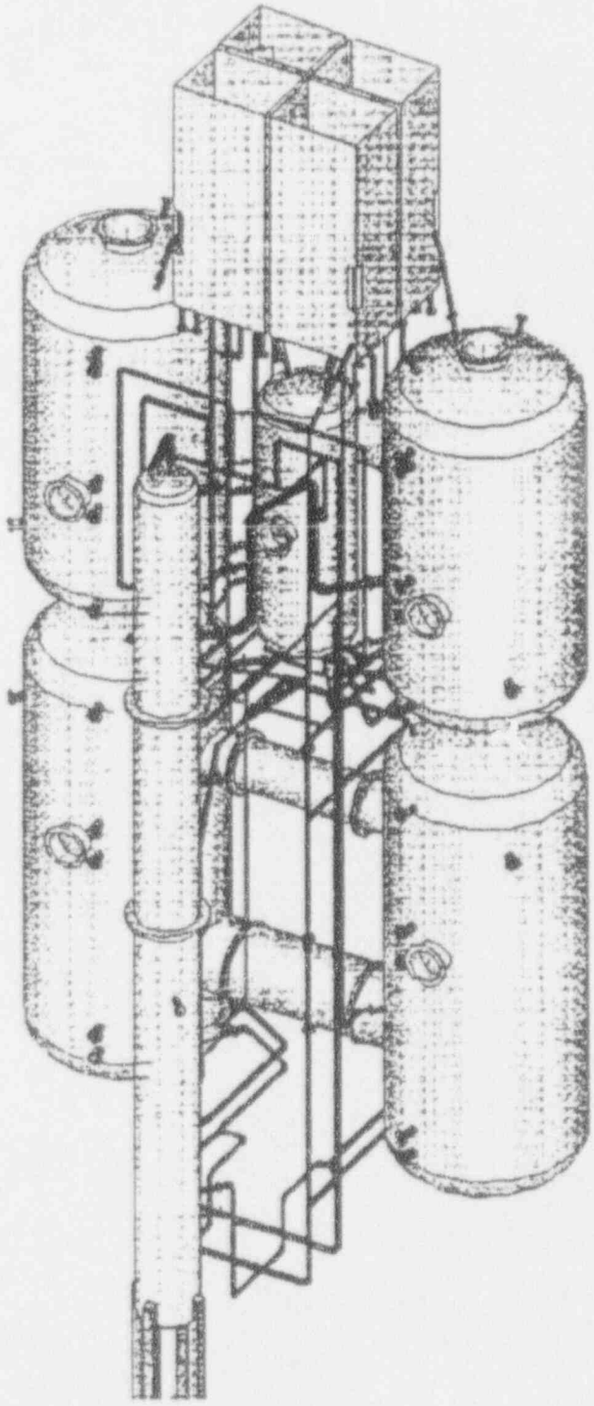

Figure 4-6 Isometric View of the PANDA Test Facility

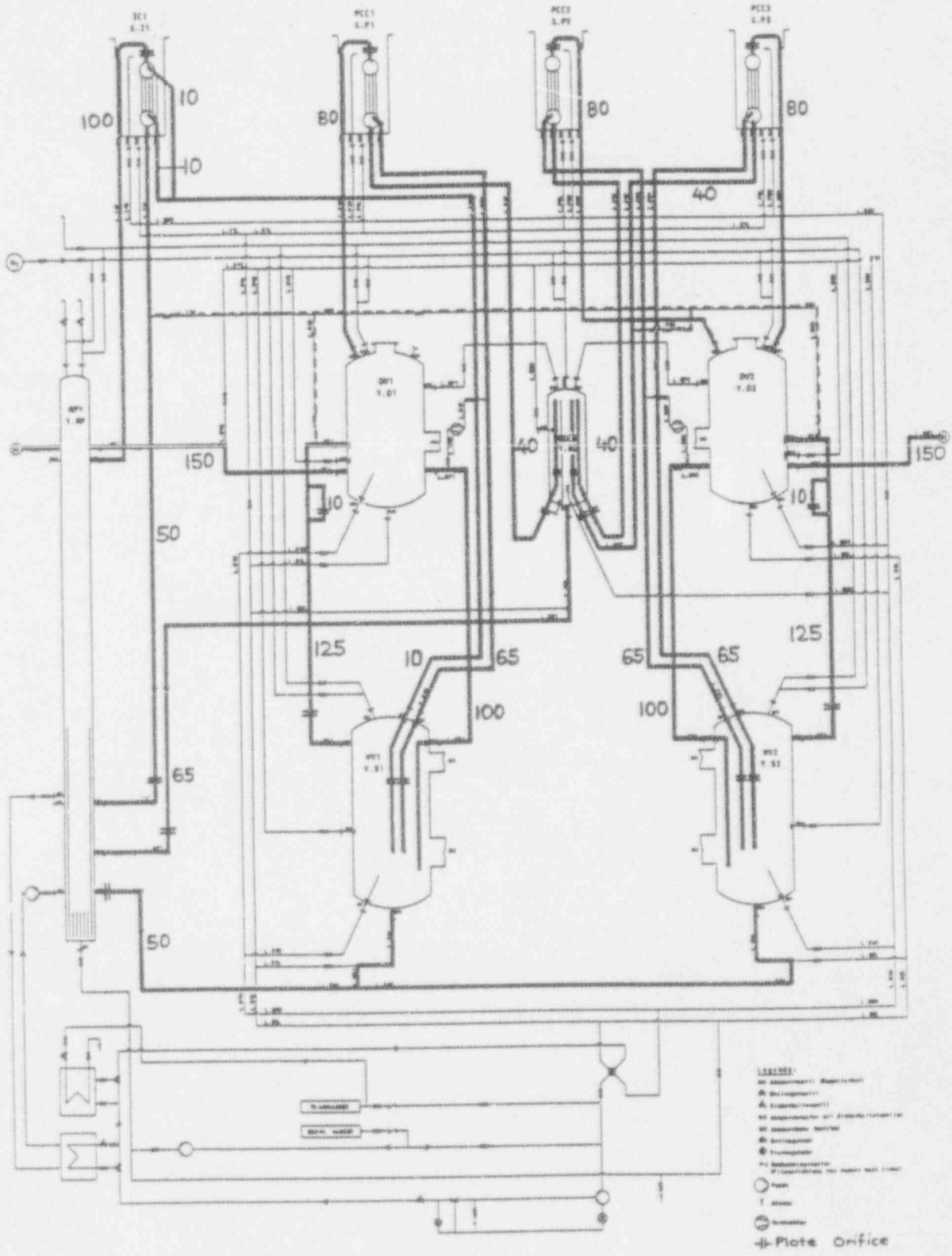

Figure 4–7 Piping Connections and Process Lines of the PANDA Facility

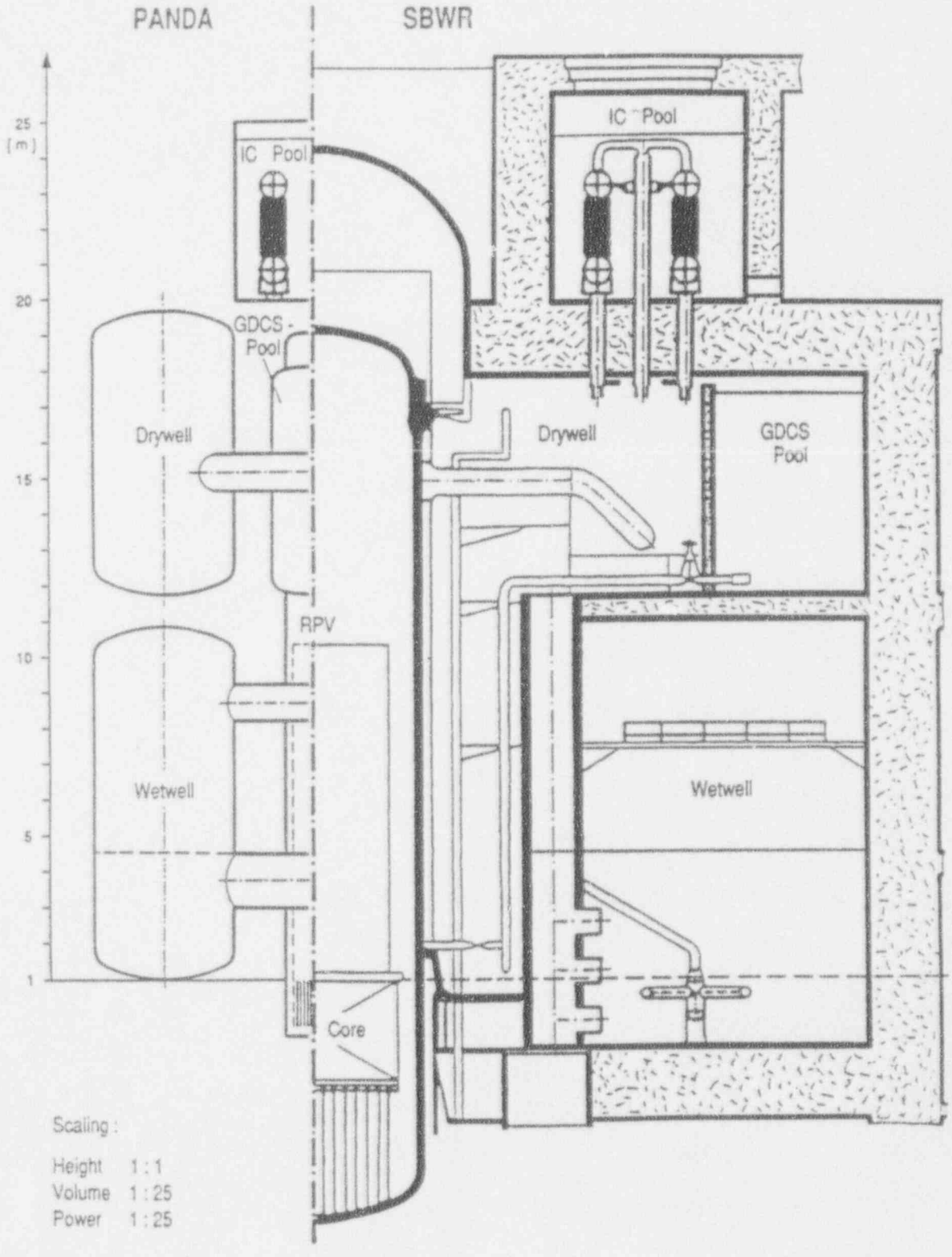

Figure 4–8 Comparison of the PANDA Elevations with the SBWR

The PANDA RPV includes a downcomer and a riser above the heater rods which represent the reactor core. The flow areas in the downcomer, the riser, and the core are scaled according to the top–down criteria of Section 2 (areas proportional to the system scale). The PANDA riser has no vertical partitions; its diameter is close to the hydraulic diameter of one partition of the SBWR riser. There is no representation of the steam separators and driers, because liquid entrainment and RPV to DW pressure drop are insignificant for the portion of the post–LOCA transients simulated by PANDA.

The *lower part of the water inventory in the SP* was eliminated to reduce vessel size; this water will not participate in the system thermal–hydraulic transient during the long–term cooling phase of the accidents considered. Indeed, the important phenomena will take place *above* the submergence depth of the PCCS vents. The PANDA PCCS vent lines are submerged in the SP with at least 2 m clearance above the bottom of the SC vessel, so that the reduced depth of this vessel will not influence venting of the noncondensables. Effects such as the convection of water to the bottom of the vessel by cold plumes running down the walls (Peterson et al., 1993) are of minor importance.

There is a depth of water of 2 m below the main vent submergence depth, that can accommodate any mixing below the vents. However, a *larger* fraction of the water inventory in the SP will absorb energy from the primary system *during blowdown*. This can be considered by properly defining the test initial conditions and preconditioning of the system accordingly.

The *lower part of the annular DW volume* surrounding the RPV was not included in the *height* of the PANDA DW volume, since it was felt that possible natural circulation phenomena taking place in this annular volume (heated on one side by the RPV) could not be adequately simulated. The volume of this annular space was, however, added to the PANDA DW *volume*. During the tests, air can also be injected at a controlled rate at the bottom of the PANDA DW to simulate the slow convection of nitrogen trapped in the annular part of the SBWR DW.

The *lowest part of the SBWR DW volume* (the region below the RPV support skirt and pedestal) is not included or added to the PANDA DW volume. Indeed, the lower DW volume provides only a "repository" for noncondensable gas or water. Its effect can be simulated in the same way as for the annular DW volume (controlled injection of air). The water inventory in the lowest part of the DW is significant only from the standpoint of producing long–term evaporation which could carry noncondensable gas to the upper DW and counteract the tendency of the noncondensables to sink to the bottom of the DW. In PANDA, this effect will be simulated by the combination of a saturated pool in the DW and controlled injections of air.

The GDCS compartment volume is smaller (1:64) than the system scale (1:25), since this volume does not play an important role in the dynamics of the system. In the transients considered, it simply provides a return path for the condensate to the RPV. The GDCS volume is about sufficiently large for containing the water inventory one hour after the LOCA. The horizontal surface area of the GDCS pool is also smaller (1:64) than the system scale. Thus while any tendency of the steam to condense on the surface of the GDCS pool water will be reduced, this will also lead to a slower heatup of the GDCS water. In terms of overall energy removal, the net effect should not be very significant.

Finally, the *volume of the ICS pools* is smaller than in the SBWR; these are scaled for 24 hrs of decay heat capacity, rather than 3 days as in the SBWR. However, water can be added at a required flow rate and temperature by the facility conditioning system to compensate for the lesser initial inventory.

4.3.2.2 Scaled Models of the PCC and IC Condensers

A critical factor that led to the choice of 1:25 for the PANDA system scale was the requirement that the condenser unit secondary side behavior be representative of the prototype condensers. The PANDA condensers are "sliced" from the prototypes (Figure 4-9). Thus the circulation of the secondary coolant in a plane perpendicular to the axis of the cylindrical headers can be made very similar to that in the actual SBWR ICS pools. The units are provided with baffles, preventing entry of the flow into the bundle in the direction of the header axis. A sufficient number of tubes was provided to have at least a couple of tubes completely surrounded by other tubes. This led to five rows of tubes, twenty tubes in total, and to the 1:25 system scale. In PANDA, condenser tubes are in all respects (height, pitch, diameter, and wall thickness) prototypical (GE, 1992).

4.3.2.3 Design of the Piping and Other Connections

All **piping** is scaled according to the criteria developed in Sections 2.3 and 2.4. The pipe diameters were calculated to match the frictional and form losses of the SBWR; the resulting pipe diameters were rounded to the next larger normalized diameter. The actual pressure drops are usually dominated by form losses which depend weakly on flow velocity (or Reynolds number) and can thus be matched very well (Huggenberger, 1992, 1993b). All lines are provided with interchangeable orifice plates that can be used to further adjust the pressure losses in the system.

The flow area of the PANDA main steam lines is the sum of the SBWR MSL's *and* the DPVs. Control valves are installed in each line (one to each DW) to simulate the different break geometries.

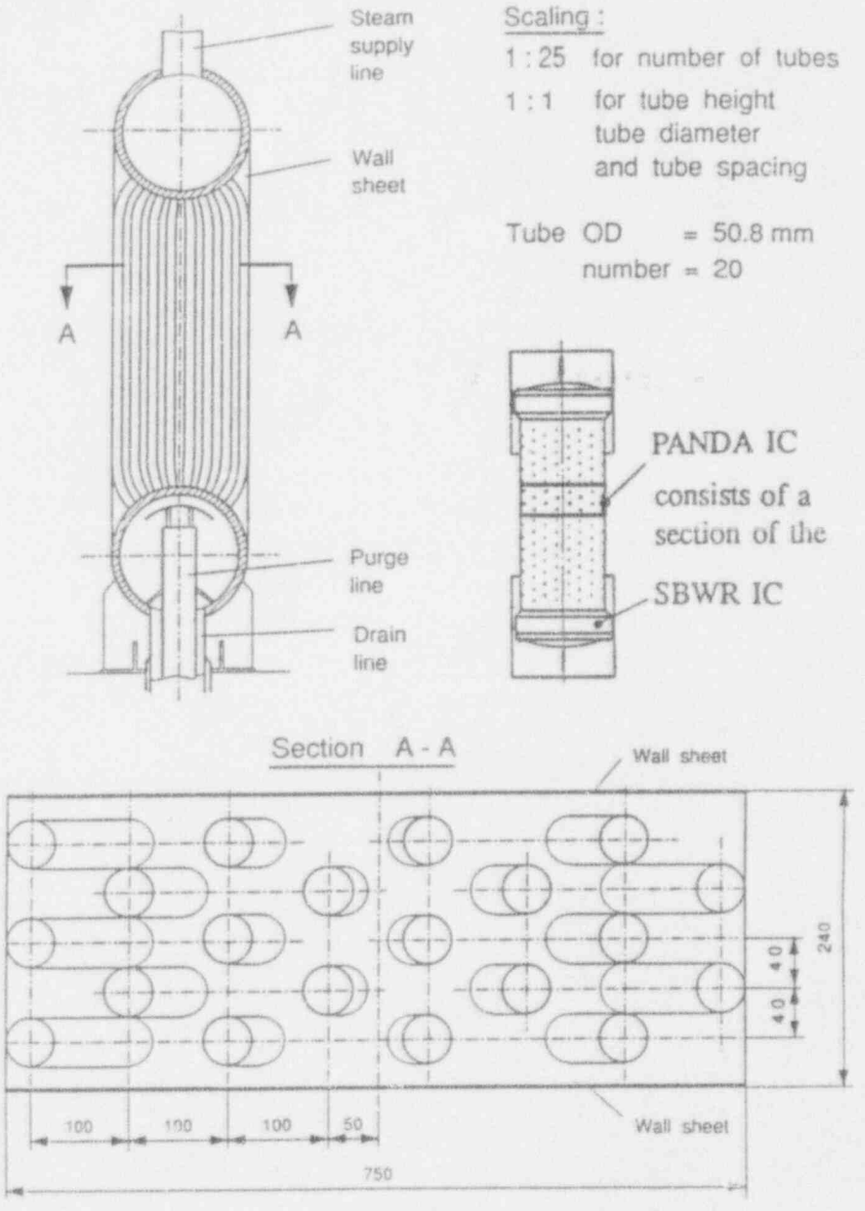

Figure 4–9 The PANDA PCCS and ICS Condenser Units

The **vacuum breakers**, which provide the flow path for potential redistribution of noncondensable gas between the SC and the DW, are simulated by programmable control valves which can reproduce the characteristics of the corresponding SBWR components. The scaling of the flows emerging from the vacuum breakers in relation

to stratification in the DW was discussed in Section 3.2.3.

Finally, the **vents** are designed according to the criteria developed in Section 3.5. In PANDA, the vertical-pipe sections of the main vents have a cross-sectional area smaller than the one dictated by the system scale. However, they are not expected to open during the experiments. The gas velocities in the main vents are in both the prototype and the model low enough to eliminate worries about dynamic effects modifying system behavior, if the vents were to open.

4.3.2.4 Heat Capacity and Heat Losses

The simulation of the heat capacity of the various SBWR structures was contemplated during the design phase of the PANDA facility. The PANDA vessels have thin walls and therefore very limited heat capacity. One could have inserted "heat capacity slabs" *in* the vessels to match the heat capacity of the SBWR structures. Use of appropriate layers of different materials *could* have provided the necessary time response. The idea was not implemented, however, since heat soaking in the SBWR structures during the long-term containment cooling period of interest is estimated to be of the same order of magnitude as the heat losses from the experiment. The heat capacity and heat loss aspects of the facility will be addressed by computation and use of calibration results during data reduction and analysis.

The PANDA vessels are very well insulated and the heat losses were conservatively estimated (for a 0.3 MPa saturated system) to be less than 4 % of the decay heat level one hour after shutdown and less than 9 % of the 24-hr-after-shutdown level (GE-PSI, 1991). More recent and more accurate estimates show that the actual losses will be significantly lower (Aubert, 1993).

The vessel internal and external wall temperatures are measured at 42 points (Dreier, 1993). This allows to determine accurately both the heat stored in the vessel walls and the heat losses. Heat loss calibration tests will be performed during commissioning of the facility. The information from these tests will be used to construct a heat-loss model of the facility. The data from the wall thermocouples will be used as inputs to the model to calculate the heat stored in the vessel walls and the heat losses during the tests; both are relatively small and both will be known with good accuracy. The heat-loss model of the facility will also be used for the code assessment analyses using the experimental data.

4.3.3 Establishment of the Proper Initial Conditions for the Tests

The PANDA facility will be equipped with auxiliary air and water supply systems for preconditioning the contents of the various system components; these are also

shown in Figure 4–7. In particular, all vessels are provided with both top and bottom filling ports and drains or vents. Thus, the possibility of establishing stratified initial conditions in the water space of the vessels at the beginning of the tests is assured.

There is also the possibility of varying the submergence depth of the vents and of the initial water level in the SP. In particular, this water level can be positioned below, at, or above the location of the large pipe connecting the two SP in the SC vessels.

In summary, all the top–down and bottom–up scaling criteria derived in Sections 2 and 3 were applied properly in designing the PANDA facility. Any deviations from these (e.g., elimination of non–active fluid inventories) were discussed in this section. The PANDA model is essentially a 1:25 "vertical slice" of the SBWR. The heat capacity and heat losses of the experimental facility cannot be made to match those of the SBWR. This issue can be addressed, however, during data reduction by an accurate system heat balance based on measurements and heat loss calibrations.

4.4 PANTHERS Tests

PANTHERS is a full scale test under prototypical flow, pressure, temperature, and non–condensable–fraction conditions of a prototypical single module of an IC condenser (half unit) and of a full PCC condenser. The PANTHERS test facility and the planned tests are described by Masoni et al. (1993).

The purpose of the tests is to qualify the proposed condenser designs regarding structural integrity and steady–state thermal–hydraulic performance. Figure 4–10 shows the schematic of the PANTHERS test facility, as it will be configured for both types of tests.

The operation of the PCCS as part of the SBWR can be described as a slow transient. Under certain conditions, its operation may become cyclical, but the period of the cycles will be long in comparison to the response time of the PCCS. The characteristic response time of the PCC condenser unit is mainly determined by the transit time of the fluid in the tubes (which is of the order of seconds), and to some extent by the time constant of the tube wall; since these walls are thin, this time constant is also of the order of a few seconds. Thus the response of the PCC condenser units to changes in inlet conditions is much faster than the response of the large SBWR containment volumes. In terms of the discussion of Section 2.4.1

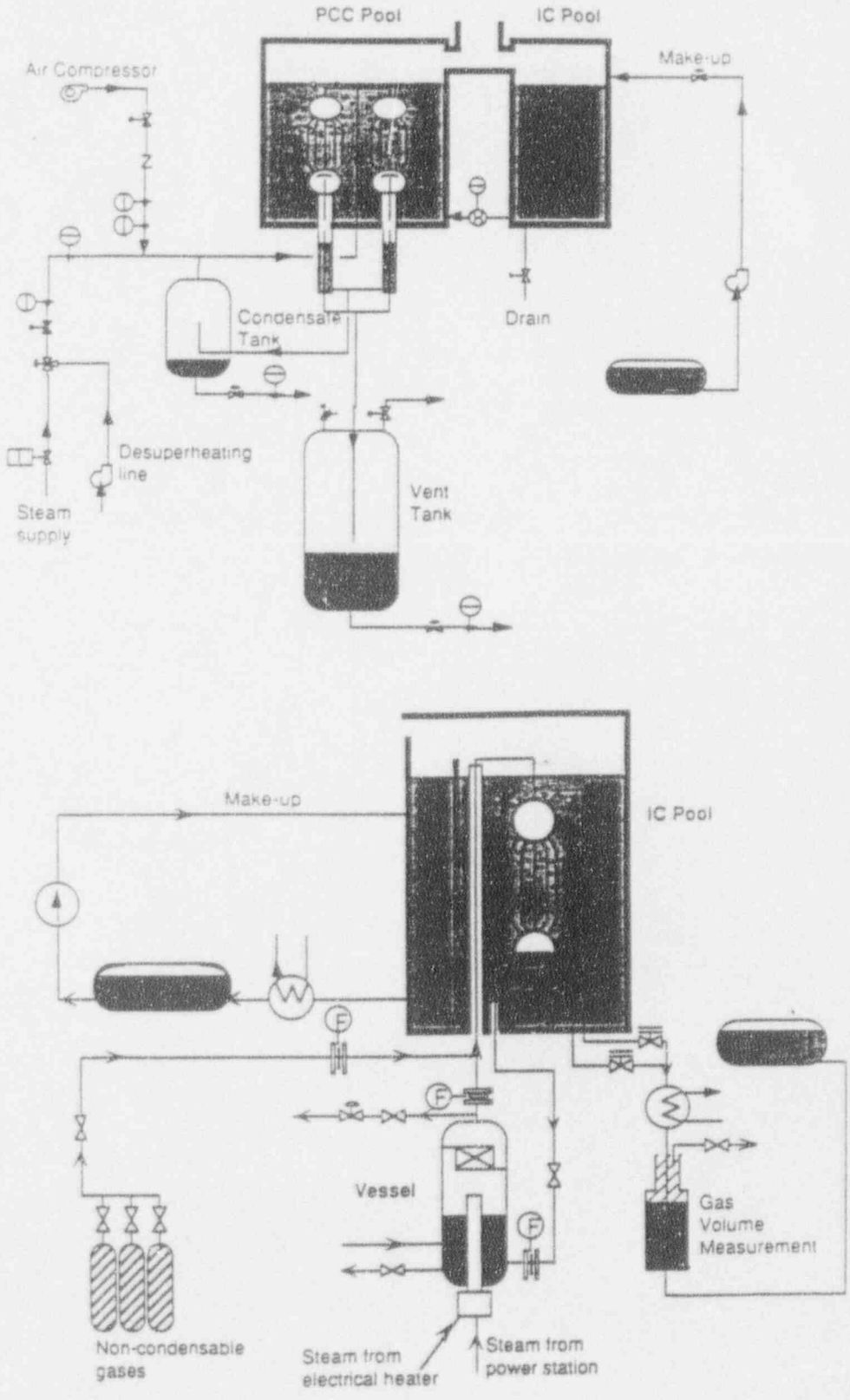

Figure 4–10 Schematics of the PANTHERS Test Facility [Top: PCC Tests; Bottom: IC Tests]

this can be expressed as $\tau^{o} \gg \tau^{o}_{tr,tubes}$. Thus the *steady state* PANTHERS tests provide adequate data to characterize the operation of the PCCS condenser units.

Some local heat flux data will also be obtained from these multi–tube units. Special care was used (Masoni et al., 1993) in installing thermocouples on both sides of the tube wall to reduce the relatively large error inherent in such measurements.

Since the PANTHERS tests are conducted with full–scale components (i.e., a prototypical PCC complete condenser unit and a symmetric one–half of an IC condenser unit), there are no scaling distortions to be addressed. There is no expected effect of testing only one half of the IC unit (one module), except possibly some influence on circulation in the pool.

The PCC condensers are installed in pools having the same dimensions as the SBWR IC pools. For the IC condenser tests, the pool surface is reduced by introducing a diaphragm wall to maintain the same area per module. Although this affects partly the boundary conditions regarding natural circulation in the pool (introduces a wall instead of a symmetry condition on one side of the unit), the effect should be minimal. In any case, small changes in the circulation patterns on the secondary side are not expected to have much influence on overall heat transfer, as discussed in Section 3.6.2.

The IC pools will be well mixed by natural circulation. The condensers are located at prototypical elevations in the pools. Furthermore, since the lower parts of the condenser units are located not much above the bottom of the pools, the entire pool water inventory will participate in the mixing process. Any unlikely stratification will be easily detected by the PANTHERS pool thermocouples.

Finally, note that any distortions due to testing only one module (half unit) will become apparent in the PCC condenser tests; for these, both a single module (half PCC unit) and the full PCC unit (two modules) will be tested.

5. References

Alamgir, Md., Andersen, J.G.M., Yang, A.I., and Shiralkar, B. (1990), "TRACG Prediction of Gravity–Driven Cooling System Response in the SBWR/GIST Facility LOCA Tests," *Trans. ANS, 62*, 665–668.

Andersen, J.G.M. et al. (1993a), "TRACG Qualification," Licensing Topical Report, NEDE–32176P, Class 3 (February 1993).

Andersen, J.G.M. et al. (1993b), "TRACG Qualification," Licensing Topical Report, NEDE–32177P, Class 3 (February 1993).

Arai, K. and Nagasaka, H. (1991), "Analytical Study on Drywell Cooler Heat Removal Performance of a Passive Containment Cooling System," pp. 281–288, paper b.4, in *Proc. 1st JSME–ASME Int. Conf. on Nuclear Engineering, ICONE–1*, Tokyo.

Arai, K., Kataoka, K., and Nagasaka, H. (1993), "TRAC Analysis of Passive Containment Cooling System Performance," pp. 143–150, Vol. 1, in *Proc. 2nd ASME–JSME Nuclear Engineering Joint Conf.*, 21–24 March 1993, San Francisco, CA.

Aubert, C. (1993), Personal communication, PSI.

Billig, P.F. (1989), "Simplified Boiling Water Reactor (SBWR) Program Gravity–Driven Cooling System (GDCS) Integrated Systems Test – Final Report," GE Nuclear Energy Report GEFR–00850 (Class II), DRF A00–02917 (October 1989).

Billig, P.F., James, A.J., and Lumini, E. (1992), "SBWR Passive Core and Containment Cooling Test Programs," paper to be presented at ANP 92, Tokyo.

Boucher, T.J., diMarzo, M., and Shotkin, L.M. (1991), "Scaling Issues for a Thermal–Hydraulic Integral Test Facility," 19th Water Reactor Safety Information Meeting, Washington, DC, October 30, 1991.

Boyack, B. et al. (1989), "Quantifying Reactor Safety Margins – Application of Code Scaling, Applicability, and Uncertainty Evaluation Methodology for a Large–Break, Loss–of–Coolant Accident," NUREG/CR–5249 (1989).

Bugg, J.D. and Rower, R.D. (1992), "Bubbling Regimes at the Wellhead of a Subsea Oilwell Blowout," pp. 571–576 in *Proc. of the 11th Int. Conf. on Offshore*

Mechanics and Arctic Engineering — 1992, 1992-OMAE, S.K. Chakrabarti et al. (editors), Vol. 1, Part B, ASME.

Chen, C.J. and Rodi, W. (1980), *Vertical Turbulent Buoyant Jets, A Review of Experimental Data*, HMT, The Science and Applications of Heat and Mass Transfer, Vol. 4, Pergamon Press, Oxford.

Clift, R. et al. (1978), *Bubbles, Drops and Particles*, Academic Press.

Coddington, P. (1992), "PANDA: Specification of the Physical Parameter Ranges, and the Experimental Initial Conditions," PSI Internal Report TM-42-92-18, ALPHA-213 (13 October 1992).

Coddington, P. (1993a), "A Procedure for Calculating Two-Phase Plume Entrainment and Temperature Rise as Applied to LINX and the SBWR," draft Internal Report, Paul Scherrer Institute.

Coddington, P. (1993b), "Review of the SBWR PCCS Venting Phenomena - Draft," PSI Internal memorandum TM-42-93.

Coddington, P., Huggenberger, H., Guentay, S., Dreier, J., Fischer, O., Varadi, G., and Yadigaroglu, G. (1992), "ALPHA - The Long-Term Passive Decay Heat Removal and Aerosol Retension Program," pp. 203-211 in *Proc. of the Fifth Int. Topical Meeting on Reactor Thermal Hydraulics, NURETH-5*, 21-24 September 1992, Salt Lake City, Utah, American Nuclear Society.

Davidson, J.K. and Harrison, D. (1963), *Fluidised Particles*, Cambridge University Press, London.

Dreier, J. (1992), "PANDA Versuchsanlage. Pflichtenheft für Messung, Steuerung und Regelung," PSI Internal Report TM-42-92-21, ALPHA 217.

Dreier, J. (1993), Personal communication, PSI.

Fannelop, T.K. and Sjoen, K. (1980), "Hydrodynamics of Underwater Blowouts," AIAA 8th Aerospace Sciences Meeting, 14-16 January 1980, Pasadena, CA, AIAA paper 80-0219.

Fitch, J.R. (1993), "Release of RPV Stored Metal Energy as a Function of Time," presented at the GE-PSI ALPHA review meeting, 14-17 September 1993.

GE (1987), "Containment Horizontal Vent Confirmatory Test, Part I," General Electric Co. Report NEDC-31393 (March 1987).

GE (1992), "PCCS Condenser Prototype General Arrangement," SBW5280DMNX1105, Rev. 1, April 7, 1992 and "IC Prototype General Arrangement," SBW5280DMNX1106, Rev. 1, April 7, 1992.

GE (1980), General Electric Company BWR/6 Nuclear Island Design, Docket No. STN 50-447 (March 1980), Amendment 1 through 21.

GE-PSI (1991), Information presented during PSI-GE Design Review Meeting, Oct. 30-31, 1991, San Jose.

Gebhardt, B., Jaluria, Y., Mahajan, R.L., and Sammakia, B. (1988), *Buoyancy-Induced Flows and Trasport*, Hemisphere Publ. Corp., Cambridge.

Huebner, M.F. (editor) (1985), *Proceedings: American Nuclear Society Meeting on Fission-Product Behavior and Source Term Research*, 15-19 July 1984, Snowbird, Utah, EPRI Report NP-4113-SR (July 1985).

Huggenberger, M. (1991a), "PANDA Experimental Facility - Conceptual Design," PSI Internal Report AN-42-91-09 (18 July 1991).

Huggenberger, M. (1991b), "PANDA Experimental Facility - Scaling of Power, Vessel Volumes and Number of IC Tubes," PSI Internal Report AN-42-91-05 (15 May 1991).

Huggenberger, M. (1992), "PANDA Experimental Facility - SBWR Data Base for the PANDA Piping Layout," PSI Internal Report AN-42-92-10, ALPHA-207 (13 October 1992).

Huggenberger, M. (1993a), "PANDA Experimental Facility. Final Conceptual Design," PSI Internal Report in preparation.

Huggenberger, M. (1993b), "PANDA System Line Scaling," Internal document, ALPHA project meeting, 13-15 January 1993.

INEL, Idaho National Engineering Laboratory (1989), "Quantifying Reactor Safety Margins," NUREG/CR-5249, EGG-2552.

Ishii, M. and Kataoka, I. (1983), "Similarity Analysis and Scaling Criteria for LWR's Under Single-Phase and Two-Phase Natural Circulation," NUREG/CR-3267 (ANL-83-32).

Ishii, M. and Zuber, N. (1970), "Thermally Induced Flow Instabilities in Two-Phase Mixtures," *Proc. 4th Int. Heat Transfer Conf.*, Paris, France, paper B5.11.

JAPC et al. (1990), "Joint Study Report, Feature Technology of Simplified BWR (Phase I), 2nd Half of 1990, Final Report," Report by the Japan Atomic Power Company and partners (November 1990).

Kiang, R.L. (1985), "Scaling Criteria for Nuclear Reactor Thermal Hydraulics," *Nucl. Sci. and Eng., 89*, 207–216.

Kim, H.T., Marquino, W., Paradiso, F.M., and Fitch, J.R. (1993), "Application of TRACG Model to SBWR Licensing Safety Analysis," Licensing Topical Report, NEDE-32178P, Class 3 (February 1993).

Kocamustafaogullari G. and Ishii, M. (1984), "Scaling Criteria for Two-Phase Flow Loops and their Application to Conceptual 2x4 Simulation Loop Design," *Nucl. Tech., 65*, 146–160.

List, E.J. (1982), "Turbulent Jets and Plumes," *Ann. Rev. Fluid Mech., 14*, 189–212.

Marriot, P.W. (1993), May 7, 1993 Letter from P.W. Marriot to R. Borchardt, Standardization Project Directorate, MFN No. 071-93, Docket STN 52-004.

Masoni, P., Botti, S., and Fitzsimmons, G.W. (1993), "Confirmatory Tests of Full-Scale Condensers for the SBWR," pp. 735–744, Vol. 1, in *Proc. 2nd ASME-JSME Nuclear Engineering Joint Conf.*, 21–24 March 1993, San Francisco, CA.

Meier, M. (1992), "Computer Model of a Passive Containment Cooling Condenser Tube," Semester Project, Nuclear Engineering Laboratory, Swiss Federal Institute of Technology.

Meier, M. (1993), communication presented at the GE-PSI ALPHA review meeting, 14–17 September 1993.

Milgram, J.H. (1983), "Mean Flow in Round Bubble Plumes," *J. Fluid Mech., 133*, 345–376.

Moody, F.J. (1986), "Dynamic and Thermal Behavior of Hot Gas Bubbles Discharged into Water," *Nucl. Eng. and Design, 95*, 47–54.

Moody, F.J. (1990), *Introduction to Unsteady Thermofluid Mechanics*, John Wiley & Sons, New York.

Mross, J.M. (1989), "Final Test Report: Testing of the Gravity-Driven Cooling System for the Boiling Water Reactor," GE Nuclear Energy Report NEDO-31680

(July 1989).

Nagasaka, H., Yamada, K., Katoh, M., and Yokobori, S. (1991), "Heat Removal Tests of Isolation Condenser Applied to a Passive Containment Cooling System," pp. 257-263, paper b.1, in *Proc. 1st JSME-ASME Int. Conf. on Nuclear Engineering, ICONE-1*, Tokyo.

NRC (1987), "Mark III LOCA-Related Hydrodynamic Load Definition," Nuclear Regulatory Commission Report NUREG 0978 (August 1984).

Ogg, D.G. (1991), "Vertical Downflow Condensation Heat Transfer in Gas-Steam Mixtures," M.Sc. thesis, University of California at Berkeley.

Paradiso, F.M., Yang, A.I., and Sawyer, C.D. (1993), "SBWR Loss-of-Coolant Accident Analysis," pp. 313-318, Vol. 1, in *Proc. 2nd ASME-JSME Nuclear Engineering Joint Conf.*, 21-24 March 1993, San Francisco, CA.

Paul, D.D. et al. (1985), "Radionuclide Scrubbing in Water Pools — Gas-Liquid Hydrodynamics," *Proceedings: American Nuclear Society Meeting on Fission-Product Behavior and Source Term Research*, 15-19 July 1984, Snowbird, Utah, EPRI Report NP-4113-SR (July 1985).

Peterson, P.F., Schrock, V.E., and Greif, R. (1993), "Scaling for Integral Simulation of Mixing in Large, Stratified Volumes," *NURETH 6, Proc. Sixth Int. Topical Meeting on Nuclear Reactor Thermal Hydraulics*, 5-8 Oct. 1993, Grenoble, France, Vol. 1, pp. 202-211.

Rao, A.S., Sawyer, C.D., and McCandless R.J. (1991), "Simplified Boiling Water Reactor Design," paper b.6, in *Proc. 1st JSME-ASME Int. Conf. on Nuclear Engineering, ICONE-1*, Tokyo.

Saha, P., Ishii, M., and Zuber, N. (1976), "An Experimental Investigation of the Thermally Induced Flow Oscillations in Two-Phase Systems," *J. Heat Transfer, 98*, 616-622.

Schrock, V.E. (1992), "Condensation Inside Tubes with Noncondensable Gas Present," USNRC-GE meeting on SBWR Passive Containment, Rockville, MD, May 29, 1992.

Schrock, V.E. (1993), Personal communication.

Schwartzbeck, R.K. and Kocamustafaogullari, G. (1988), "Two-Phase Flow-Pattern Transition Scaling Studies," *ANS Proceedings, 1988 National Heat Transfer*

Conference, 24–27 July 1988, Houston, Texas, pp. 387–398.

Shiralkar, B.S., Alamgir, Md., and Andersen, J.G.M. (1993), "Thermal Hydraulic Aspects of the SBWR Design," to be published.

Siddique, M. (1992), "The Effects on Noncondensable Gases on Steam Condensation Under Forced Convection Conditions," Ph.D. thesis, Dept. of Nuclear Engineering, Massachusetts Institute of Techology.

Siddique, M., Golay, M.W., and Kazimi, M.S. (1989), "The Effect of Hydrogen on Forced Convection Steam Condensation," *AIChE Symp. Ser.*, *85* (No. 269) 211.

Siddique, M., Golay, M.W., and Kazimi, M.S. (1993), "Local Heat Transfer Coefficients for Forced-Convection of Steam in a Vertical Tube in the Presence of a Noncondensable Gas," *Nucl. Technology*, *102*, 386–402.

Smith, B., Dury, T.V., Huggenberger, M., and Nöthiger, H. (1992), "Analysis of Single-Phase Mixing Experiments in Open Pools," pp. 101–109 in *Proc. ASME Winter Annual Meeting*, Anaheim, CA.

Upton, H.A., Cooke, F.E., Sawabe, J.K. (1993), "Simplified Boiling Water Reactor Passive Safety Features," pp. 705–712, Vol. 1, in *Proc. 2nd ASME-JSME Nuclear Engineering Joint Conf.*, P.F. Peterson (ed.).

Vierow, K.M. (1990), "Behavior of Steam-Air Systems Condensing in Cocurrent Vertical Downflow," M.Sc. thesis, University of California at Berkeley.

Vierow, K.M. (1993), "GIRAFFE Passive Heat Removal Testing Program," GE Nuclear Energy Report NEDC-32215P, Class 3 (June 1993).

Vierow, K.M. and Schrock, V.E. (1991), "Condensation in a Natural Circulation Loop with Noncondesable Gases. Part I – Heat Transfer," *Proc. of the Int. Conf. on Multiphase Flows '91 Tsukuba*, 24–27 September 1991, Tsukuba, Japan, Vol. 1, pp. 183–190.

Vierow, K.M., Fitch, J.R. and Cooke F.E. (1992), "Analysis of SBWR Passive Containment Cooling Following a LOCA," *Proc. Int. Conf. on the Design and Safety of Advanced Nuclear Power Plants*, 25–29 October 1992, Tokyo, Japan, Vol. III, pp. 31.2.1–7.

Wallis, G.B. (1969), *One-Dimensional Two-Phase Flow*, McGraw-Hill Book Co, New York.

Yadigaroglu, G. and Bergles, A.E. (1972), "Fundamental and Higher-Mode Density-Wave Oscillations in Two-Phase Flow," *J. Heat Transfer, 94*, 189-195.

Yokobori, S., Nagasaka, H., Tobimatsu, T. (1991), "System Response Test of Isolation Condenser Applied as a Passive Containment Cooling System," pp. 265-271, paper b.2, in *Proc. 1st JSME-ASME Int. Conf. on Nuclear Engineering ICONE-1*, Tokyo.

Yokobori, S., Tobimatsu, T., Ohta, M., Kurita, T. and Nagasaka, H. (1993), "System Response Test of PCCS Performance Considering Drywell-Wetwell Leakage," pp. 683-690, Vol. 1, in *Proc. 2nd ASME-JSME Nuclear Engineering Joint Conf.*, P.F. Peterson (ed.).